8-2002

Application of Raman Techniques for Paper Coatings

Shivashanker Bitla

APPLICATION OF RAMAN TECHNIQUES FOR PAPER COATINGS

By

Shivashanker Bitla

B.S. University Department of Chemical Technology (UDCT), India, 2000

A THESIS

Submitted in Partial Fulfillment of the

Requirements for the Degree of

Master of Science

(in Chemical Engineering)

The Graduate School

The University of Maine

August, 2002

Advisory Committee:

Carl P. Tripp, Associate Professor of Chemistry, Co-Advisor

Douglas W. Bousfield, Professor of Chemical Engineering, Co-Advisor

William J. Desisto, Assistant Professor of Chemical Engineering

APPLICATION OF RAMAN TECHNIQUES

FOR PAPER COATINGS

By Shivashanker Bitla

Thesis Co-Advisors: Dr. Carl Tripp, Dr. Douglas Bousfield

An Abstract of the Thesis Presented
in Partial Fulfillment of the Requirements for the
Degree of Master of Science
(in Chemical Engineering)
August, 2002

Paper coatings are mixtures of pigments, binders and other additives used to improve the optical and printing properties of paper. During application, particle migration may occur resulting in a non-uniform distribution of pigments and binders. This may influence product quality. Raman spectroscopy is a potential tool to characterize coatings in terms of pigment/binder and pigment/pigment distribution. However, there is little work reported on this topic.

Various coatings were applied to model substrates, dried and analyzed with Raman spectroscopy. $CaCO_3$ pigment and Styrene Butadiene latex binders are easy to detect and monitor in paper coatings when kaolin clays are not present. Raman spectroscopy can detect the subtle differences between Ground Calcium Carbonate (GCC) and Precipitated Calcium Carbonate (PCC). The different morphologies of $CaCO_3$,

Calcite and Aragonite, can be distinguished and quantified using Raman spectroscopy. Procedures to record and calibrate $CaCO_3$ pigment-SB latex binder and Calcite-Aragonite coating color mixtures were developed. Dry blends of the components to record spectra produce good calibration curves.

We investigate the particle migration with various particle sizes of pigments and binders. For pigment/binder systems, binder migration depends on the pigment/binder size ratio and not on the absolute concentration of binder in the coating color. Similar results are observed with pigment-pigment systems. A critical size ratio of three is found that determines if particle migration will occur or not. A dissolved polymer in the system is found to reduce migration.

Raman spectroscopy can quantify the contribution of the non-uniformity in the spatial composition of the paper coatings to various print defects such as mottle. Large binder/pigment compositions contribute to low density of pigmented ink applied with a contact device. This result must be from low local absorption of ink in that region.

ACKNOWLEDGMENTS

I would like to extend my utmost appreciation to my advisors Dr. Douglas Bousfield and Dr. Carl Tripp for their guidance and encouragement throughout this research. Special thanks to Dr. Carl Tripp for teaching me different aspects of Raman spectroscopy. I would also like to thank Dr. William Desisto for spending his time and energy for benefit of my thesis.

I would like to thank University of Maine Paper Surface Science Program for funding this research. Also I would like to thank the Laboratory for Surface Science and Technology (LASST) for the assistance and support.

I would like to thank Basant Dimetry for helping me in preparing the coatings, Dr. Sofian Kanan for helping me with Raman spectroscopy, Seongnam Ahn and Dr. Yang Xiang for teaching me different aspects in coatings and Sungiai Jeon for letting me use his samples. I would also like to thank all graduate students and staff of chemical engineering and LASST for their support throughout the two years.

Finally I would like to thank my parents, my sister and brother-in-law for their loves, without their support, I couldn't finish this work.

TABLE OF CONTENTS

LIST OF TABLES

LIST OF FIGURES

Chapter 1

INTRODUCTION

1.1 Paper Coating

Paper is often coated to improve the print quality attributes along with smoothness and opacity of the sheet. Conventional paper coatings consist of pigment particles with a binder such as starch or latex. Today, about one-half of all papers used in the printing industry are coated. Coated papers find widespread usage in books, magazines, and advertising materials.

Coatings are applied on the paper surface as an aqueous suspension of pigments and binders in soluble or particulate form. The aqueous phase is removed by drainage into the sheet and by evaporation. At the end of this process, a dry coating structure is formed consisting of a non-uniform mixture of pigments, binders, and voids. The pore structure has a strong influence on the paper optical, mechanical and fluid absorption properties[1].

When the aqueous phase drains into the base sheet, various components may move relative to others[2]. This movement could alter the printing, physical or optical properties of coated sheet. Non-uniform absorption into the paper may cause non-uniform coating properties. However, the conditions that cause relative movement of components are not well understood and tools to characterize this phenomenon are not in place. This thesis will address this point.

1.2 Pigments

The pigment particles are the building blocks of the final coated layer, and as a result, their role is of the utmost importance. In the wet state the pigments typically constitute greater than 80% of the total formulation, with the remaining 20% being the binder and various additives. Different types of pigments are used in order to confer some desired property to the finished product (i.e. gloss, printability, smoothness). The performance of a specific pigment depends on a multitude of both physical and chemical properties such as chemical composition, particle morphology, refractive index, and reactivity. Kaolin and calcium carbonate are the most commonly used pigments. Other pigments include titanium dioxide (rutile and anatase), amorphous silica, talc, calcium or barium sulfate[3].

1.2.1 Calcium Carbonate

$CaCO_3$ is one of the major pigments in paper coating industry. In 2000, 69% of the total European-based coatings used $CaCO_3$[4]. A major reason for this is it's low cost. There are two main types of calcium carbonate ($CaCO_3$) pigments used in paper coatings: ground calcium carbonate (GCC) and precipitated calcium carbonate (PCC) [5, 6]. GCC directly comes from the natural calcium carbonate deposits, such as chalk, marble, limestone[4] and are ground to a very fine size through several mechanical processes. Coarser grades of GCC are used in pre-coat, base coat or size press formulation while fine ones are suitable for topcoat. The particle size and shape makes it possible to use these pigments at high levels and high coating solids without rheology or runnability problems in high-speed blade coaters. PCC is formed through a chemical process but also

starts with the use of natural calcium carbonate deposits. First, the natural calcium carbonate deposits are calcined to produce calcium oxide (CaO) and carbon dioxide gas (CO_2). The calcium oxide is then reacted with water under controlled conditions to yield a calcium hydroxide slurry ($Ca(OH)_2$). The calcium hydroxide slurry is then screened to remove any unreacted lime or other impurities. Then carbon dioxide gas is bubbled through the calcium hydroxide slurry to form precipitated calcium carbonate ($CaCO_3$).

The advantage of the chemical process is that it provides a means of controlling both size and morphology of the pure calcium carbonate pigment. PCC's typically have large surface area and therefore generally have higher oil absorption than the ground limestone. The particle shape and size of the PCC are determined by precipitation conditions such as rate, concentration, temperature, type and degree of agitation, and the use of additives. By carefully controlling precipitation conditions, calcite, aragonite or a mixture of the two pigments can be obtained[5].

As a coating pigment, $CaCO_3$ can achieve a bright, white coating more economically than clay and it is extensively used in wood-free offset grades as a pre-coat and in applications where the coat is required to have good ink absorption and receptivity. Since its chunky particles also develop gloss less readily than the laminar particles of Kaolin clay, it has advantages as a pigment in matt (non-glossy) grades. The superior particle packing of $CaCO_3$ pigments, as compared to kaolin particles, dismisses their use for gravure printed grades.

There are subtle differences in the properties imparted to paper coatings for GCC verses PCC. Natural GCC produces easier drainage and drying of the paper web and

shows a lower size demand, a more closed sheet structure and higher paper strength; while PCC based coatings provide higher light scattering[5].

1.2.2 Kaolin

Kaolin is also a widely used pigment in paper industry. In 2000, 31% of the total European-based coatings used kaolin[4]. Structurally, kaolin is a 1:1 layered aluminosilicate that consists of a tetrahedral silica surface and an octahedral alumina surface. The theoretical structural formula of kaolin is $Al_2O_3 \bullet 2SiO_2 \bullet 2H_2O$, and has a theoretical composition of 46.5% SiO_2, 39.5% Al_2O_3, and 14% H_2O[7]. Kaolin is a natural, mined pigment and is classified as coming from either primary or secondary deposits. Primary deposits are found in close association with the parent rocks, and therefore have a high proportion of other minerals and impurities, which must be removed before the kaolin is ready for coating applications. On the other hand, secondary deposits have been transported, by water, away from their original source, and consist of mainly beds of pure clay.

In paper coating applications kaolin finds widespread use in the wood-containing sector, especially for lightweight coated grades (LWC) [7]. The sheet-like atomic structure of kaolin produces flat plate-like pigment particles, which allow coated gloss to be achieved readily. Also, since the particle packing behavior of these plate-like particles is quite poor, the resulting coating is quite bulky and open. This produces a compressible coating layer which is advantageous in the gravure printing process. The compressible nature of the kaolin coating enables good contact to be made with the ink contained in the recessed cavities of the gravure printing cylinder.

1.2.3 Titanium Dioxide

Titanium dioxides, both rutile and anatase, which have a high refractive indexes, are often used to improve the brightness of paper coatings. It is a synthetic pigment, and as such is probably the most expensive ingredient used in paper coating formulations. There are two common procedures used for the manufacture of TiO_2 pigments. In the first process, the "sulfate process", the ore ilmenite ($FeO \bullet TiO_2$) is leached with sulfuric acid, and the resulting solution is subsequently hydrolyzed. The hydrated product is then calcined at high temperature to form titanium dioxide. In the second process, the "chloride process", the ilmenite is reacted with carbon and a chlorinating agent. The titanium tetrachloride that is formed is heated in a stream of air at high temperature to produce TiO_2[7].

1.3 Binders

The primary purpose of binder is to hold the pigment particles together and to anchor the coating to the surface of the paper. The binders fall into two classes, natural and synthetic products. The natural binders include starch, such as cornstarch and potato starch, and proteins, such as casein. Synthetic binders include styrene-butadiene latex, acrylic latex, polyvinyl alcohol, polyvinyl acetate, photographic gelatins, vinylidene chloride polymers, and carboxymethylcellulose[3]. Latex binders are usually about 0.1 μm in diameter. Typically, the binder level in the paper coating is about 10~20 parts on 100 parts of pigments and these vary depending on the binder type and desired final paper coating properties.

1.4 Additives

Although 99% of the coating is pigment, binder and water, the remaining 1% additives in the paper coatings are very important. The general functions of additives is to make the basic coating color compatible with the raw stock and the coating equipment, and to provide control of foaming, lubricity, crosslinking, rheology and water retention[8]. Some examples of additives includes polyphosphate, alkali silicates and alkali polyacrylates as dispersants; sodium alginate, carboxymethylcellulose (CMC), hydroxyethylcellulose (HEC), and polyarylates as Water Retention and Rheology Modifiers (WRRMs) [8].

1.5 Chemical Analysis of Paper Coatings

The coating structure has a very strong influence on the paper optical, mechanical and fluid absorption properties[1] and therefore, paper coatings are often analyzed by their physical or mechanical properties such as coating color viscosity, coat weight, water adsorption rate on coating and coating porosity. However, chemical analysis of paper coatings is equally important because many print quality issues are determined by ink interactions with the coating components, binder /pigment distribution in the paper coating and pigment binder interactions. A knowledge of the chemical composition is found necessary in controlling the papermaking operation, in judging suitability of the product for a specific application, in estimating behavior during use which may be dependent on chemical composition, for detection of undesirable or deleterious impurities, in meeting established specifications, in determining origin or source, and in

evaluating competitive products[3]. Also, the physical properties are linked to the chemical composition of the coating.

In most cases, the coating chemical composition is known from the quantities and types of ingredients used in the coating formulation. However, the distribution and composition uniformity of the coating can vary and has an impact on print quality. Thus, there is a clear need to develop analytical tools that can spatially identify the chemical composition of paper coatings. One of the earliest chemical analytical techniques involved mechanical scraping of individual layers of the coating (0.5~0.8 μm) using a blade[9-13]. Using standard chemical methods to measure binder in the scraped coating powders, the binder concentration at different depth level on the paper coating was measured[11-13]

The development or application of new analytical techniques in recent years has led to significant advances in determining the chemical distribution in coatings. These techniques include spectroscopic methods such as Attenuated Total Reflectance (ATR) Infrared Spectroscopy[14-16], Photoacoustic FT-IR Spectroscopy[17, 18], and Ultraviolet Absorption (UV) [19-21]. The absorption spectroscopic techniques are typically fast, nondestructive and easy to use. UV absorption has limited use to the analysis of unsaturated binder material, such as styrene butadiene latex. Infrared techniques are rich in informational content and can be used to identify binders and pigments. However, the infrared light penetrates deep within the paper leading to high opacity due to absorption by water and the wood fibers. Furthermore, there is poor spatial and depth resolution using either UV or IR spectroscopic techniques.

High vacuum microscopy techniques, such as Electron Probe Micro Analysis (EPMA)[22, 23], X-ray photoelectron spectroscopy (XPS)[10, 23-25], Secondary Ion Mass Spectrometry (SIMS)[24-27], and Laser Induced Plasma Spectrometry (LIPS)[28-30] have also been applied to paper analysis. Typically, vacuum based electron techniques require tedious sample preparation and provide chemical analysis over large areas. XPS is surface sensitive, providing chemical information only on the first 5nm. But XPS is difficult to analyze different binders due to contribution of all binders to C_{1s} band. Laser ablation techniques such as LIPS, provide depth resolution but suffer from thermal mixing and the same limitation of binders as XPS. Above all, differentiation between different organic binders is difficult by electron beam techniques[10].

Other techniques include Scanning Electron Microscope (SEM)[31-35]and Atomic force microscopy (AFM)[35, 36], which gives the topographic information of paper coating surface, X-ray Fluorescence Spectroscopy[37],which is used to measure the coating weight, Nuclear Magnetic Resonance (NMR)[38-40], which measures the pore size or porous structure of the paper coatings.

1.6 The Raman Effect

Raman spectroscopy is a potentially new technique for analyzing paper coatings. The Raman effect results from the interaction of light and matter. The scattering of light can be classified as elastic (Rayleigh) or inelastic (Raman). In the former case the scattered light is observed at the same frequency as the incident light. On the other hand, inelastically scattered light, which is detected at different frequencies, constitutes the Raman spectrum of the sample[41].

The inelastic scattering of light by matter was predicted on theoretical grounds by Brillouin[42] in 1922 and by Smekal[43] in 1923. The first experimental observation of the inelastic scattering of light was made by Raman and Krishnan in 1928[44]. A complete semi-classical theory of the Raman effect was published a few year later[45]. The spectroscopic application of the Raman effect made relative little progress, until the invention of the laser[46, 47]. And the first use of laser as excitation source in Raman spectroscopy appeared in 1962[48, 49]. Through the following years, a considerable number of instrumental developments were made.

1.6.1 Mechanism of the Raman Effect

The Raman effect results from the induced vibrational and/or rotational motions of molecules with the electromagnetic radiation. According to quantum theory, a molecular motion can have only certain discrete energy states. A change in state is thus accompanied by the gain or loss of one or more quanta of energy. A quantum of energy is defined by

$$\Delta E = h\nu_k ,$$

where h is Planck's constant and ν_k is the classical frequency of the molecular motion. The interaction of a molecule with electromagnetic radiation can thus be analyzed in terms of an energy-transfer mechanism.

Scattering processes involve at least two quanta acting simultaneously in the light-matter system. Simple elastic scattering occurs when a quantum of electromagnetic

energy if created at the same time that an identical one is annihilated. Thus, the molecule is unchanged by the event. In the case of an inelastic process such as the Raman effect, the two photons are not identical and there is a net change in the state of the molecule. If, for example, the created photon is less energetic than the annihilated one, the scattered light is observed at a frequency that is lower than that of the incident light. This case is referred to as Stokes Raman scattering. On the other hand, if the created photon is the more energetic of the two, the Raman frequency will be higher than that of the laser and the anti-Stokes spectrum will be produced.

The scattering processes described above are illustrated in Figure 1. The laser excitation at frequency ν_0 reappears as the relatively strong Rayleigh line. The much weaker Raman 'sidebands' are the result of inelastic scattering by a molecular vibration of frequency ν_v. These scattering processes are very weak. Typically, the intensity of the Rayleigh line is about 10^{-3} with respect to the incident excitation, while the Raman features are at least another factor of 10^{-3} weaker. The combined effect is that Raman scattered radiation is at least 10^{-6} weaker than the incident excitation[41].

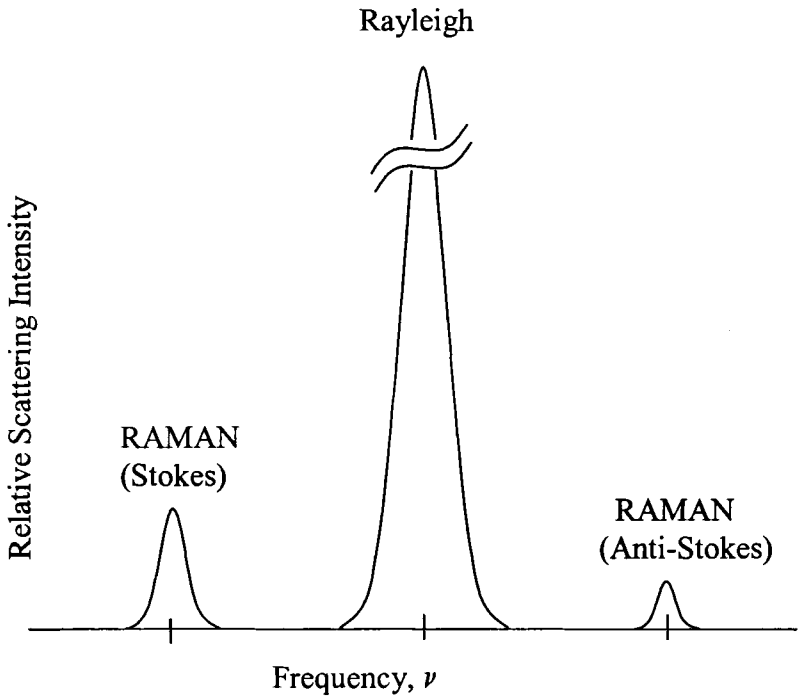

Figure 1.1. Raman and Rayleigh scattering of excitation at a frequency ν_0. A molecular vibration in the sample is of frequency ν_v.

Usually, the Raman frequencies are measured relative to that of the excitation $\pm\nu_v$, and quoted as values of inverse wavelength, expressed in cm^{-1}.

$$\bar{\nu}_v = \nu_v / c = 1/\lambda_v,$$

Where λ_v is the corresponding wavelength.

1.6.2 Difference Between Raman and Infrared

Infrared spectroscopy (FT-IR) is another technique that provides molecular vibration/rotation information. The two techniques, FT-IR and Raman spectroscopy, are complementary to each other. In most of cases, the strong Raman bands (molecular vibrations/rotations) are weak in the infrared and, in the opposite direction, strong infrared bands are weak in the Raman spectrum. The difference comes from the fundamental difference in the mechanisms of the interaction between molecules and incident light.

Infrared adsorption occurs when the incoming radiation interacts with the oscillating permanent dipole of the molecule. For Raman scattering, as discussed above, the incident radiation induces a dipole change in the molecule. Thus infrared adsorption requires a permanent dipole whereas Raman scattering arises from an induced dipole in the molecule and this is related to the polarizability of the molecule. This leads to different selection rules for bands and a complete vibrational analysis requires the collection of both the infrared and Raman spectra.

1.6.3 Raman Spectroscopic Analysis of Paper Coating

The use of Raman spectroscopy for analysis of paper coatings has several advantages over other spectroscopic and high vacuum techniques. As with absorption spectroscopic methods, there is little sample preparation and Raman spectroscopy is fast and nondestructive. It can be used in water-based system whereas these measurements are difficult when using the complementary infrared vibrational technique because water is very strong IR absorber but weak Raman scatterer. However, the information content is

as rich as infrared spectroscopy and in paper coatings, exceeds that of its infrared counterpart. For example, Raman spectroscopy is better at distinguishing between differing crystalline structures. This information can be used to study pigment-pigment interaction between different crystalline structures.

The main disadvantage that has prevented widespread usage of Raman spectroscopy has been the presence of fluorescence in many samples. The Raman effect is a weak effect with about 1 in 10^6 photons undergoing a Raman shift[41]. This contrasts to fluorescence quantum yields of near unity. Typically the fluorescence from the presence of small amounts of impurities can easily swamp and mask out the much weaker Raman signal. Thus, the presence of fluorescence due to impurities had limited Raman spectroscopy to very pure laboratory based materials. This limitation has been circumvented with recent instrumental developments. Fluorescence has been avoided by using lasers operating below the fluorescence manifold in the far-red region of the spectrum. Developments with red frequency diode lasers and red sensitive CCD array detectors have made Raman spectroscopy accessible to almost any material regardless of purity. Furthermore, the sensitivity of Raman spectrometer has greatly improved with notch filter developments enabling the use of single monochrometers coupled with red sensitive CCD arrays detectors. The combined improved sensitivity and fluorescence-free capability now enable industrially based paper coatings to be analyzed with ease.

Measurements of latex content on the coating surfaces and the pigment-latex distribution on the x-y scale using Raman spectroscopy is reported by Pei He (PSSP group, University of Maine, 1998-2000) and others (Vyorikka J., VTT) in the literature. However, paper coatings' high scattering properties has prevented the use of

conventional confocal Raman techniques. Confocal Raman spectroscopy coupled with immersion sampling method is being developed to study the depth profiles in coating layers[50].

In this thesis, I report the use of Raman spectroscopy to detect the differences between GCC and PCC and distinguish different crystalline forms of $CaCO_3$ namely Calcite and Aragonite for quantitative analysis. Pigment and binder migration under various conditions is reported for Aragonite-Calcite and $CaCO_3$-SB latex systems respectively. Quantification of non-uniform spatial composition contribution to print mottle generation for pigmented inks is also reported.

Chapter 2

EXPERIMENTAL

2.1 Raman Spectroscopy

Raman spectra were collected using a Renishaw Raman Imaging Microscope System 1000. It is a compact laser Raman microprobe/microscope system that can collect both Raman spectra and global Raman images. Signal detection is achieved through the use of a sensitive charge coupled device (CCD) array detector, with instrument control performed by a personal computer. The software package consists of two software suites working together, instrument control software (WiRE, Renishaw) and data analysis software (GRAMS/32®, Galactic).

2.1.1 Components of the Raman Spectrometer

This Raman system has five basic units: laser, spectrometer, microscope, CCD camera, and computer. The optical layout is shown in Figure 2.1.

The excitation source is an SDL-XC30 diode laser, SDL Inc. It operates at a wavelength of 785 nm with a maximum power output of 170~300mW at the head. The measured power at the sample position is about 35mW maximum for 50×/0.75 LEICA N PLAN objective. A 785 nm-based laser was selected because it avoids fluorescence as this wavelength lies below the electronic threshold for most samples.

The laser enters the spectrometer and passes through a neutral density filter (attenuation filter) wheel, a beam expander (located at the spatial filter position in Figure 2.1) and is reflected from a 785 nm holographic notch filter into the microscope. The

software controlled neutral density filter provides a selection of power levels at the sample. Beam expansion is performed to provide a uniform laser power density at the sample position.

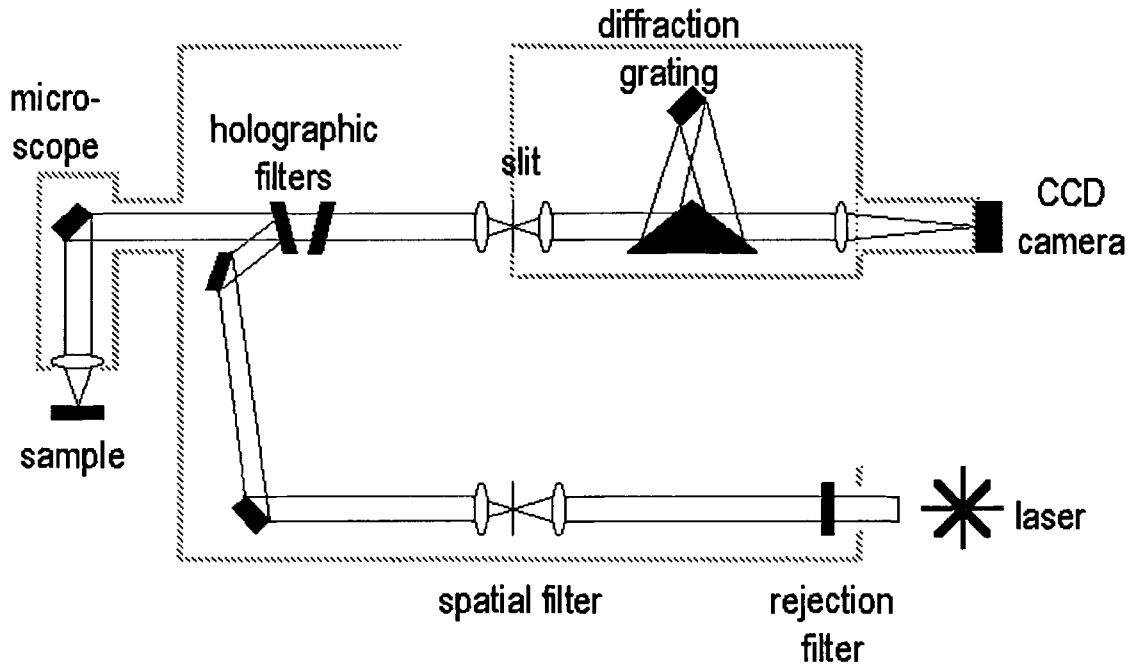

Figure 2.1. The optical system of the Renishaw Raman Microscope Imaging System 1000.

The microscope, LEICA DM LM from Leica Mikroskopie und Systeme GmbH, consists of an eyepiece, an image camera (CCD-IRIS, SONY Inc.) connected to the computer, two white light sources (transmitted and reflected) various objectives (5×, 20×, 50×, etc.), and a automatically motorized stage. The image camera is used to capture the microscopic image as seen from the eyepiece and recorded and displayed on the computer. When performing an automatic mapping experiment, the scan area is software selected from the stored image on the computer screen. The automatic motorized stage has a 0.1 micron precision with 1 micron minimum moving step (0.5 micron in depth) in

xyz position, and can be controlled in WiRE/GRAMS/32. The objective is used to both focus and collect the 180° backscattered Raman signal. The use of a common lens for both laser focus and Raman collection provided the spatial coherence between the visual image at the center of the crosshairs and the collected Raman spectrum.

The 180° backscattered radiation collected using the objective returns to the spectrometer. This frequency-shifted signal now passes through the 785 nm holographic filter (this also serves a Raleigh line rejection filter) and is focussed by a lens through a variable slit and dispersed by a grating onto the CCD detector (see Figure 2.1).

2.1.2 Spectra Acquisition

Data acquisition and spectrometer parameters are under computer control provided through Renishaw WiRE (Windows-based Raman Environment), and the collected/manipulated data is analyzed, displayed, and stored by Galactic GRAMS/32 (Graphic Relational Array Management System).

The Raman system calibration and alignment was checked daily and whenever the system was powered on. Calibration and alignment of the Raman spectrometer was monitored using the 520.5 cm^{-1} Raman band of silicon wafer. The following experiment setup conditions were used to measure signal intensity: static collection mode, 0.5 second collection time, 100% laser power, high gain, 50× LEICA N PLAN objective, confocal slit 20 microns, CCD image 20 pixels width. Using these parameter settings a well-aligned system gave peak intensity of 15000~20000 counts, with band center at 520.5 ± 0.5 cm^{-1}.

Maximum signal intensity is obtained when the laser is focused on the sample. The focus position was determined using the white light/CCD camera combination. A fixed mirror is then rotated into position which blocks the white light beam and deflects the laser beam on the sample.

2.1.3 Spatial Resolution

The spatial resolution for our Raman spectroscopy depends on the system conditions, parameters, and sample properties (for the depth resolution). Typically, under the following conditions (50× microscopy objective, 2 microns confocal slit width, and 4 pixels CCD image width), the spatial resolution for paper coating is 2 micron laterally and 4 microns in depth[51].

When using the 5× objective the measured spot size was approximately 20 microns in diameter.

2.2 Materials

The materials used in this study include paper coating materials and several laboratory-generated coatings.

2.2.1 Paper Coating Materials

$CaCO_3$ pigment, both Ground Calcium Carbonate (GCC) and Precipitated Calcium Carbonate (PCC), both calcite and aragonite crystal forms, Styrene Butadiene (SB) latex binder are used. $CaCO_3$ pigments are typically around 1~2 microns or less in size and contribute to 80%~90% of the total coating dry weight. SB latex binder is 0.15

microns in size and contributes to 10%~20% of the total coating dry weight. In some cases, Carboxy methyl cellulose (CMC) additive is used. Because its contribution is only ~2% in the paper coating, it is not detected in our Raman measurements.

The spectra of the pure compounds were recorded on the neat powder (about 10 mg) placed on top of a microscope slide. Some compounds were obtained as aqueous based slurries and these samples were dried and grounded before they placed on glass slides. The instrumental parameters are as follows unless stated otherwise in the figure caption: 35 mW 785 nm laser at sample collected spots, 50× microscope objective, 2 microns width of confocal slit, 4 pixels width of CCD camera. These parameters resulted in a 2 microns diameter sample area. The collection time for obtaining spectra with good signal-to-noise depended on Raman scattering intensity and this typically was about 30 seconds.

2.2.2 Paper Coatings

All the coatings were lab generated using a rod draw down coater. Coating materials were obtained from the member companies of PSSP (Paper Surface Science Program, University of Maine).

To record a Raman spectrum of a coated paper sheet, a sample (1cm×1cm square) was mounted on a microscope glass slide and it is placed in the slide holder on the automatic stage.

The following steps are involved in a lab generated paper coating.

1) Preparation of Coating mix, called coating formulation
2) Applying coating mix to the base stock, using draw down coater
3) Drying of coated sheet

In a typical preparation of paper coating formulation, pigment particles are first dispersed in water at a concentration of 70 % to form pigment slurry. Screening is followed, if necessary, to remove flocs from pigment slurry. Then binder, additives, more water (to adjust the solid content to ~65 %) is added followed by thorough mixing of the solution. The resulting solution is called 'Coating Color'. p^H is then adjusted to 8.5.

The main objective of any coating operation is to apply an even layer of coating in a controlled manner. Rod draw down coater, because of its simple operating procedure, is mostly used in laboratory to generate paper coatings. The draw down coater consists of a platform, a series of threaded rods, and a supporting stage that positions the rod above the platform attached to a small motor. Base sheet is taped to the platform. Excess coating color is placed before the stage and a speed of 1200 m/minute is applied. The stage moves applying shear on the coating color leaving a uniform film of coating mix on the base sheet which is then IR dried. Since the coating mix is contained in the valleys between the windings, the diameter of the wire is important. The larger the diameter of the wire, the deeper and wider is the valley between two windings and more of the mixture will deposit on the web, producing higher coat weights. From the known coating slurry solid concentration and density, the coating weight can be selected for each rod. Coat weight is generally expressed in terms of grams per square meter (gsm). Our lab

instrument K303 (RK Print-Coat Instruments Ltd., shown is figure 2.2) with use of # 3 rod for a 65% solid concentration produces a coat weight of about 15 gsm.

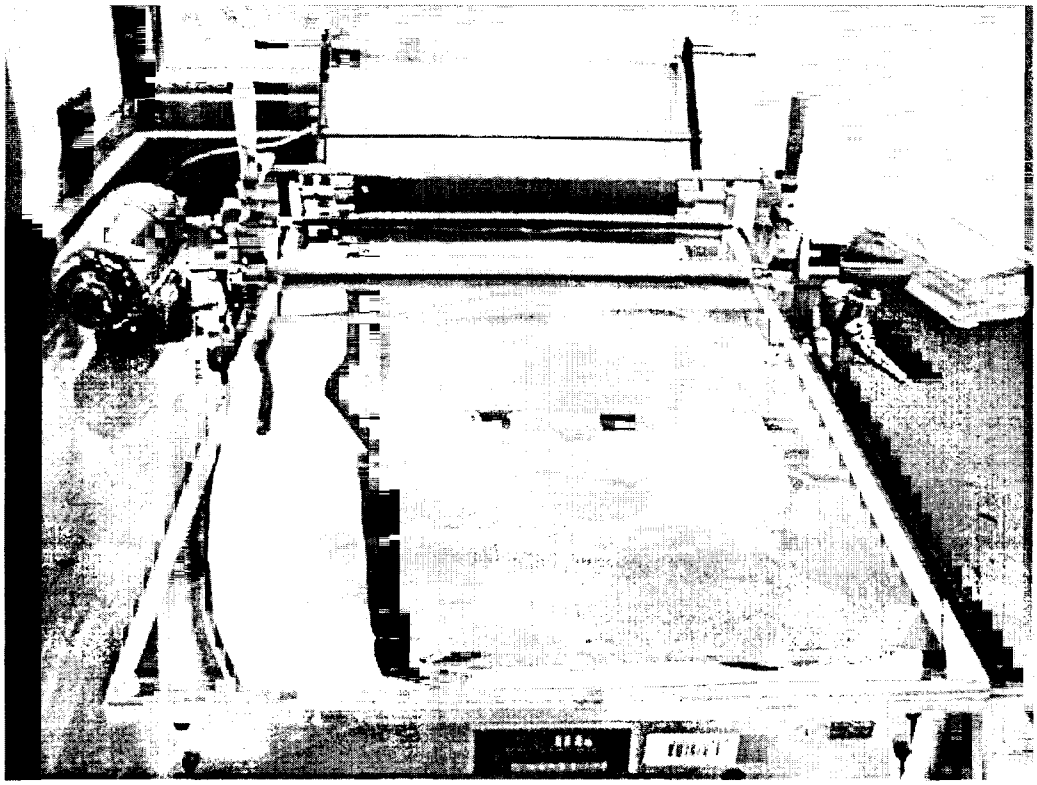

Figure 2.2 Laboratory Rod Draw down coater (K 303, RK Print-Coat Instruments Ltd.)

In a coating color preparation, all the measurements are carried out on dry weight basis and the moisture content of the components are included in the calculations with the amount of water to finally adjust the solid content. Coating color is generally expressed in terms of the parts of binder with respect to 100 parts of a pigment and a 10 pph SB in $CaCO_3$ means 10 parts of SB latex in 100 parts of $CaCO_3$ pigment which is nothing but 10 gm SB binder per 100 gm of $CaCO_3$ pigment (dry basis). For a 10 pph (parts per hundred) $CaCO_3$ coating color, the following procedure, shown in Table 2.1, is used.

Table 2.1. 10 pph SB in $CaCO_3$ Coating Color Formulation

Pigment Slurry					
	Parts	% solids	Dry wt (g)	Wet wt (g)	Water (g)
GCC	100	99.51	995.1	1000	5
To be added					190.72
Slurry		**72**	**995.1**	**1382.08**	
Coating Color					
	Parts	% solids	Dry wt (g)	Wet wt (g)	Water (g)
Pigment	100	72.5	453.12	625	172
Binder	10	50.42	45.3	89.84	44.54
To be added					51.84
Coating Mix		**65**	**498.42**	**766.8**	

In the first step, 1000 gm of $CaCO_3$ is slowly added to 190.72 gm of distilled water while stirring. The solid concentration of the pigment slurry is about 72%. This slurry is stirred for 10 minutes and then a 89.84g of 50.42 % of SB latex (DOW 620NA) is added while stirring. Then distilled water 51.84 g is added to adjust the solid content to 65%. This value was verified by drying the sample with an IR lamp followed by reweighing.

Base sheet is then taped to coater platform, and a # 3 rod is used for a 15 gsm coat weight. Coated sheet is then placed under the IR lamps for drying.

Chapter 3

RAMAN ANALYSIS OF PAPER COATINGS

3.1 Introduction

In this chapter we discuss the Raman spectra of paper coating components and characterization of paper coatings using Raman spectra. Specifically, the differences between various calcium carbonates are detectable with Raman spectroscopy and can be used to characterize the paper coatings. Calibration methods which are required for quantification of pigment-binder and pigment-pigment mixtures are also explained in this chapter. Interference due to cellulose is not observed in Raman spectra as we collected spectra from coating surfaces which are at least 15 μm in thickness.

3.2 Raman Spectra of Coating Components

Our study of coating components with Raman Spectroscopy is focused on $CaCO_3$ pigment and SB latex binder. Our experience in recording many different commercial and in-house formulated coatings has shown that identification of the additives was below our detection limit of our technique. Details of the spectra-collection methods for these coating components as well as the paper coatings are described in chapter 2.

3.2.1 Calcium Carbonate

Of all the pigments used in paper coatings, $CaCO_3$ is by far the easiest to detect and monitor in coatings. Although the two types of $CaCO_3$ (GCC- mined from natural deposits and ground to fine sizes and PCC- chemically synthesized for desired particle

size and morphology) come from two different manufacturing processes, they have similar chemical properties as well as the same crystalline calcite structures. Raman spectra of both GCC and PCC are shown in Figure 3.1. There are four major Raman bands in both $CaCO_3$ spectra locating at 1086 cm^{-1}, 712 cm^{-1}, 282 cm^{-1}, and 156 cm^{-1}. The most intense band at 1086 cm^{-1} band is assigned to the symmetric stretching vibration, v_1, of carbonate group (CO_3^{2-}) in $CaCO_3$. Also, the band at 712 cm^{-1} is the bending vibration, v_2, of the carbonate. The 282 cm^{-1} is the rotatory lattice vibration, r_1, and the 156 cm^{-1} is the translatory lattice vibration, t_1, of the $CaCO_3$ crystal. In our work, the strongest Raman band at 1086 cm^{-1} is used to quantitatively analyze $CaCO_3$ (both PCC and GCC) in paper coatings.

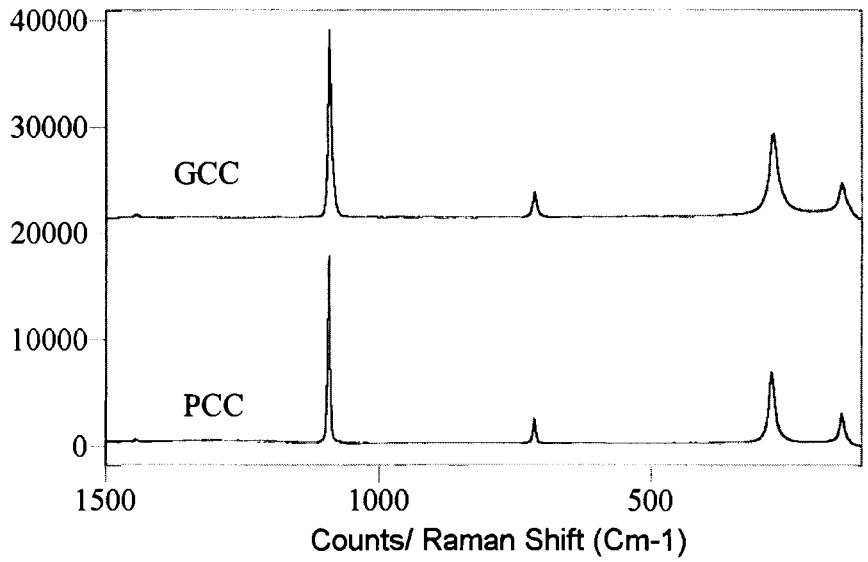

Figure 3.1 Raman spectra of GCC and PCC.

Our experience in recording spectra of various calcites has shown that there are small but notable differences between all GCC and PCCs. The PCC bands are generally

wider and shift to lower frequencies compared to those of GCC. A comparison of the band position (band maximum) and FWHM (Full Width at Half Maximum) of the four major calcium carbonate Raman bands at 156cm^{-1} 282cm^{-1} 712cm^{-1} and 1086cm^{-1}, are listed in Table 3.1.

Table 3.1 Raman Peak Maxima and FWHM of GCC and PCC.

GCC		PCC	
Peak maxima (cm^{-1})	FWHM	Peak maxima (cm^{-1})	FWHM
155.9	8.1	155.1	12.7
281.9	12.2	279.7	18.8
712.7	4.9	712.0	8.8
1086.4	4.6	1085.7	6.9

An increase in Raman band widths for a crystalline solid are due to an increase in temperature and the presence of impurities, vacancies or other imperfections in the crystal lattice, in particular, the amorphous materials have very broad features[52]. Although both PCC and GCC are crystalline solids, the PCC is more amorphous-like than GCC. PCC is made from solution through precipitating process. While crystalline in nature, PCC contains some amorphous nature and contains hydrogen-bonded water. We recall that water is used in the production of PCC and small quantities remain intercalated in this material. GCC is ground natural calcite and therefore does not have internal hydrogen bonded water. This is confirmed with IR Drift spectra, which show a broad band in the 3700-2500 cm^{-1} region due to hydrogen bonded water[53].

Other crystalline form of PCC is aragonite. For aragonite, we see identical peaks in the high frequency region (due to carbonate group) where as for lattice vibrations in the low frequency region further shift to lower value. Rotatory lattice vibrations in calcite appear at 282 cm^{-1} where as in aragonite they appear at 203 cm^{-1}. Raman spectra of aragonite and calcite are shown in Figure 3.2. These huge differences differentiated in the Raman can be utilized to study pigment-pigment systems without really going for an altogether new pigment.

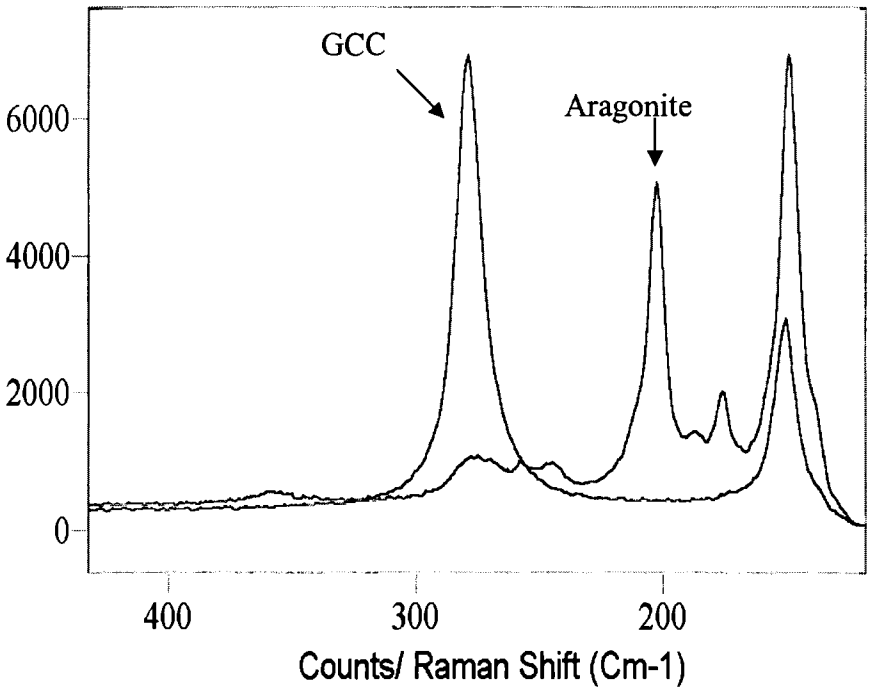

Figure 3.2 Raman spectra of lattice rotary bands of Aragonite and Calcite $CaCO_3$.

3.2.2 Kaolin

The Raman spectrum of kaolin is shown in Figure 3.3. The broad feature extending over the full spectral region is due to fluorescence from kaolin-based samples.

This fluorescence masks out the weaker kaolin Raman bands shown in the spectrum with the expanded ordinate scale in Figure 3.3 (This expanded scale spectrum was collected for 90 seconds after reduction of fluorescence by laser irradiation of the kaolin sample for one hour). In addition the spectrum was baseline corrected to remove the fluorescence background. Although the full-scale spectrum in Figure 3.3 shows a band at 144 cm^{-1}, it is due to the trace TiO_2 (anatase) in the kaolin[54].

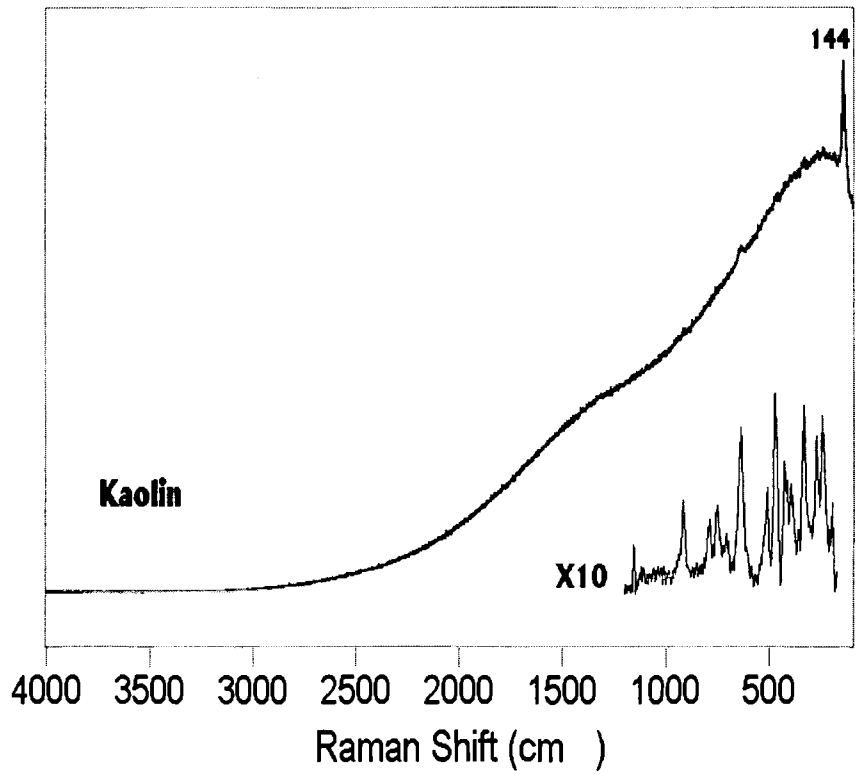

Figure 3.3 Raman spectra of kaolin. The expanded-scale spectrum from 1200 cm^{-1} to 170 cm^{-1} has been baseline corrected.

Our Raman system uses a 785 nm-based laser because this frequency lies below the fluorescence manifold for most samples and impurities. This is the case for all pigments and binders except for kaolin. The fluorescence in the kaolin is due to

impurities in the sample as long irradiation time on the same spot lowers the intensity of the fluorescence.

While we view the fluorescence in kaolin based samples as a major limitation, it is noted that we have been able to obtain quality spectra of other pigments and binders in kaolin based paper coatings, even if the kaolin content is as high as 60% in industrial paper coatings and this doesn't prevent quantification of other components in coating.

3.2.3 Styrene Butadiene Latex

The styrene butadiene latex is a copolymer consisting of styrene and butadiene monomers. The repeat units of styrene and butadiene in a copolymer are shown in the following Figure 3.4.

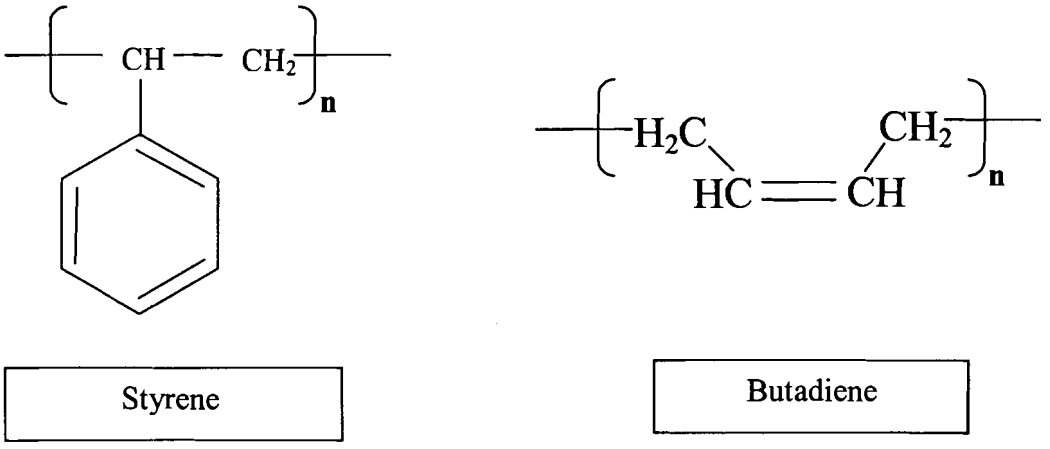

Figure 3.4 Molecular structures of styrene and butadiene repeat units in styrene butadiene copolymer[55].

Styrene butadiene latex has very strong band at 1001 cm^{-1} and is used in this work to quantitatively analyze styrene butadiene in paper coatings. Raman spectrum of SB latex is shown in the following figure 3.5. This peak corresponds to the benzene ring

symmetric stretch of the styrene component. Other bands around 1665 cm^{-1} from the unsaturated C=C bond are very weak compared to the benzene ring band.

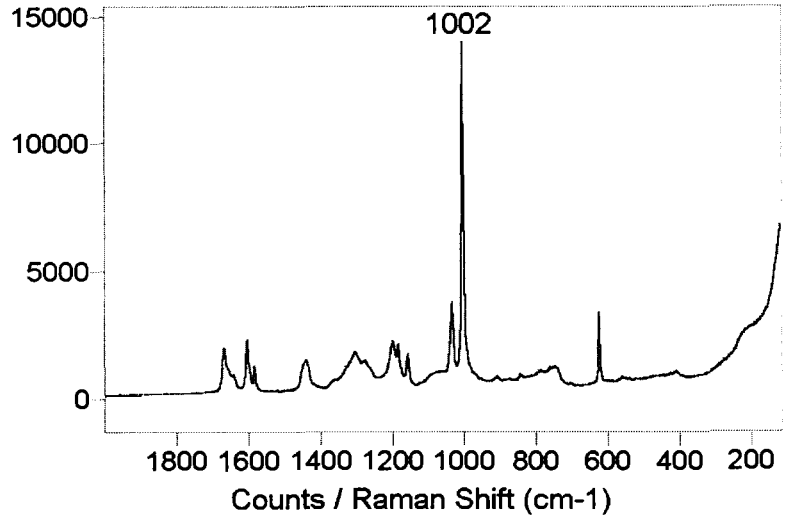

Figure 3.5 Raman spectrum of SB latex.

3.3 Quantification of Paper Components

For Raman spectra of paper coatings, a direct correlation between band intensity (or integrated intensity) with quantity of material is difficult because the intensity of band will vary due to geometric effects arising from non-uniformity in paper coating morphology, unknown scattering cross section and other less defined effects. Therefore, rather than measuring the absolute intensity of any one band, the ratio of intensity (or integrated intensity) of bands due to different components is calculated. If desired, the ratio in band intensity can be converted to a % wt ratio. In this case calibration curves are used to determine the relative amount of each component in the coating layer.

3.3.1 Characterization of $CaCO_3$-SB Coatings

The strongest bands of $CaCO_3$ at 1086 cm^{-1}, SB latex at 1001 cm^{-1} are used for quantification of $CaCO_3$-SB coatings. Collected spectra are baseline corrected and offset to zero before the ratio of SB/$CaCO_3$ intensities is calculated. The band areas for $CaCO_3$ and styrene butadiene were integrated in GRAMS/32. For $CaCO_3$ the integration area 15 cm^{-1} each side of the band centered at 1086 cm^{-1} was used. For styrene butadiene an integration area was taken from 12.5 cm^{-1} each side of the band centered at 1001 cm^{-1}. The SB/$CaCO_3$ ratio is computed from the ratio of the 1001 cm^{-1} band area (styrene butadiene) to the 1086 cm^{-1} band area ($CaCO_3$). To convert these SB/$CaCO_3$ intensities to % wt ratio, calibration curves are used. An example of the calibration curve is shown in Figure 3.6 for $CaCO_3$ and styrene butadiene. Different amounts of $CaCO_3$ and styrene butadiene latex were mixed together and dried. After thorough mixing, the blend is deposited on glass slides and Raman spectra are recorded at a 20 μm spot size. The accuracy of this measurement varies and for typical $CaCO_3$/SB coatings, we find the accuracy in the % wt ratio is about ± 5 % at the 95% confidence level. In most cases the % wt is not required for interpretation of pigment or binder migration. In this case we are interested in the change in pigment/binder composition at the surface between various coating colors and base sheets and this can be determined by monitoring the relative change in intensity of the Raman bands.

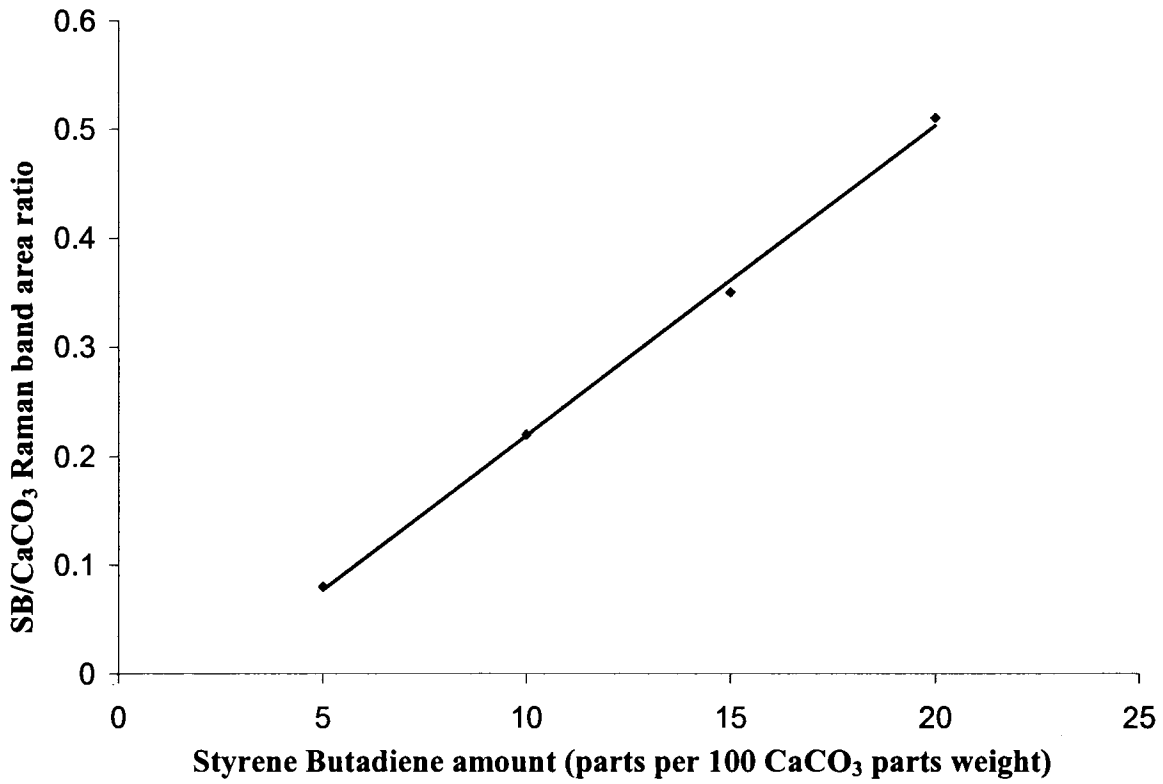

Figure 3.6 Calibration curve of styrene butadiene amounts in mixtures vs. measured $SB/CaCO_3$ Raman band area ratios.

3.3.2 Characterization of GCC-PCC Coatings

For GCC-PCC coatings, peaks at 281.9 cm^{-1} and 279.7 cm^{-1} are considered for quantification of GCC and PCC respectively. % wt of GCC or PCC is calculated for these coatings through calibration curves. To generate calibration curves, known combinations of GCC and PCC are mixed and dry blended. The Raman spectra of these mixtures is shown in the following Figure 3.7.

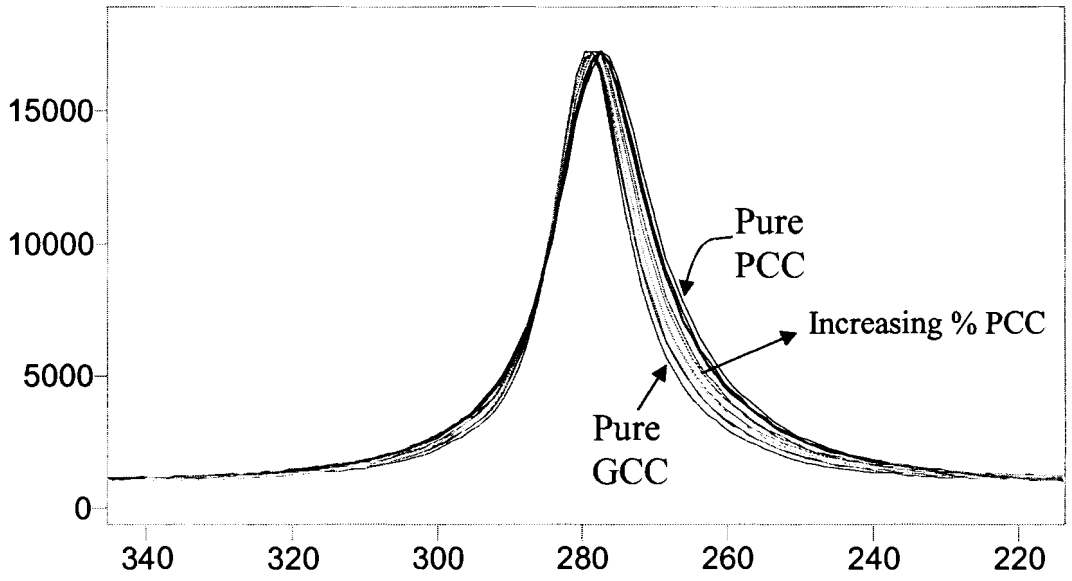

Figure 3.7 Raman spectra of coatings containing different GCC/PCC mixtures.

As the % PCC to GCC increases there is a broadening of the 282 cm^{-1} band to lower frequency. A calibration curve (shown in figure 3.8) is generated by normalizing the intensity measured at a point on the lower frequency side (269.5 cm^{-1}) to the intensity at peak maxima.

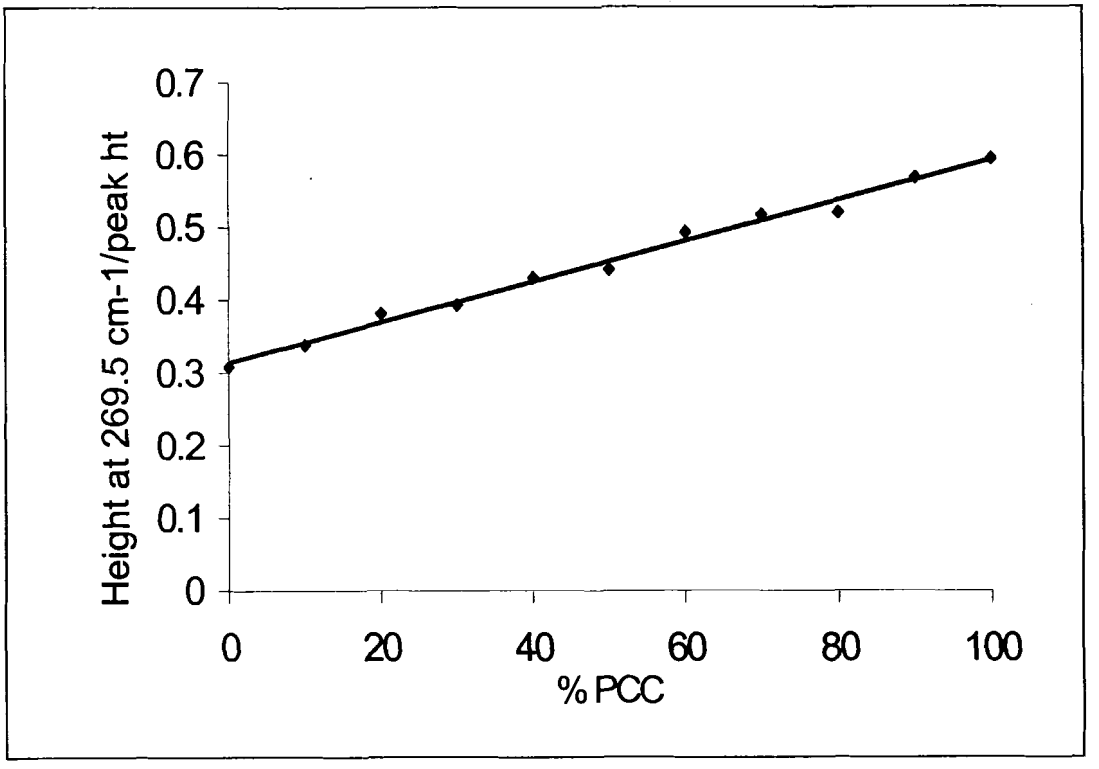

Figure 3.8 Calibration curve used to determine the % amount of PCC in a calcite coating mixture. The ordinate is computed by dividing the intensity measured at 269.5 cm^{-1} to the intensity at peak maxima.

3.3.3 Characterization of Calcite-Aragonite Coatings

Here we discuss the calibration of calcite/aragonite coatings including the collection method of the spectra. All the calcite and aragonite mixtures used in our study are obtained in slurry form. Various calibration methods were investigated and the best method for collecting the spectra is described. First the slurries are IR dried and grounded and dry blended. Various combinations of calcite and aragonite are prepared and individual bands of aragonite at 203 cm^{-1} and calcite at 282 cm^{-1} are used to calibrate the calcite-aragonite system. As shown in Figure 3.9, as the % aragonite in the mixture increases, the aragonite band at 203 cm^{-1} increases and the corresponding calcite band at

282 cm^{-1} decreases and the calibration curve obtained from the ratios of these band areas is shown in Figure 3.10.

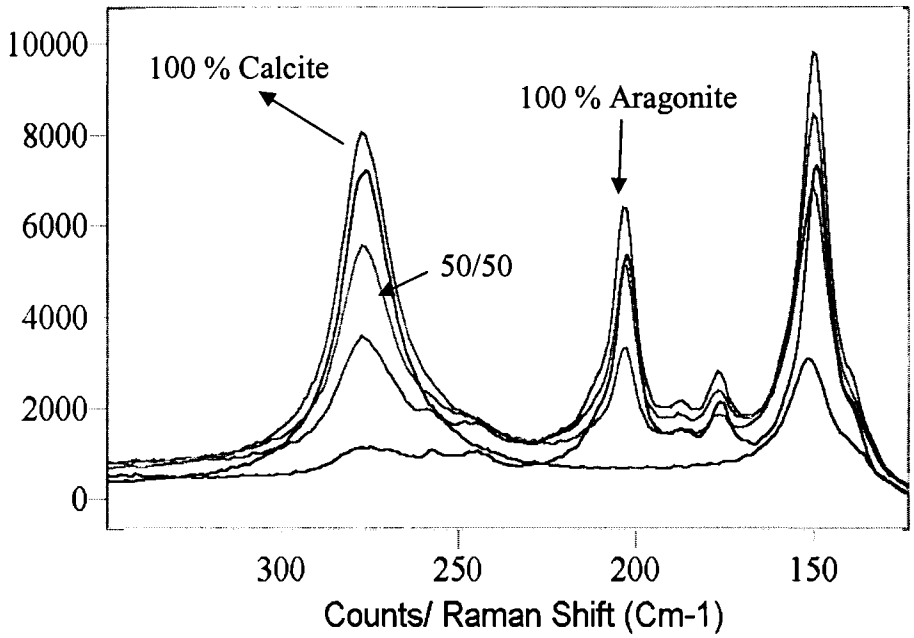

Figure 3.9 Raman spectra of coatings containing different Aragonite/Calcite mixtures.

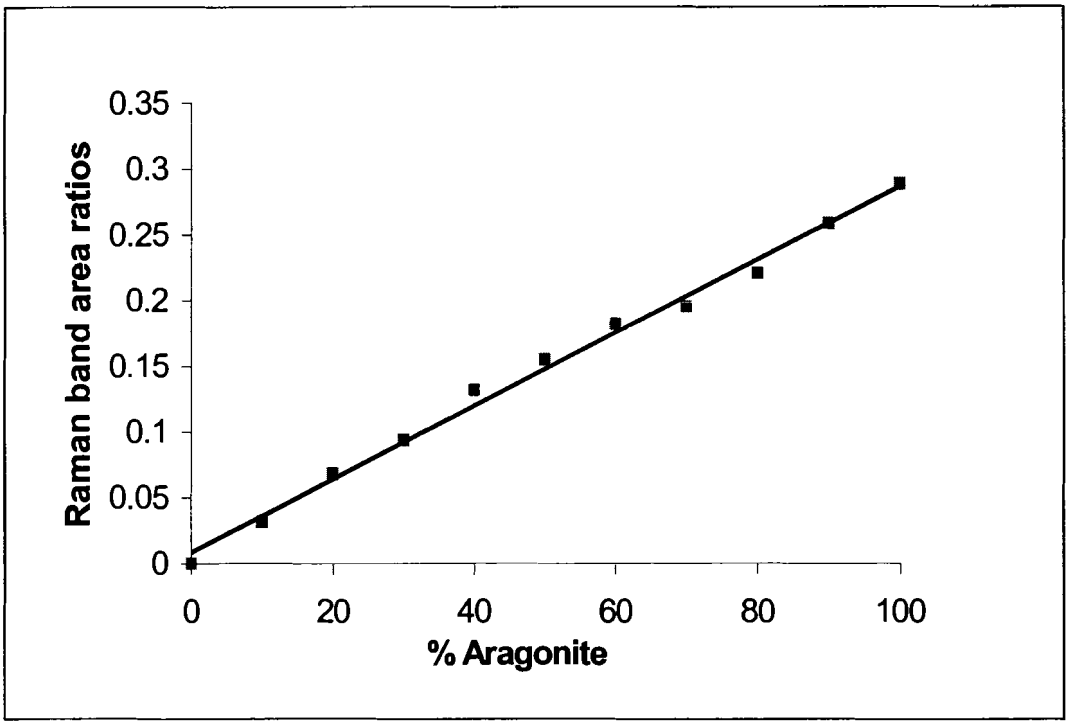

Figure 3.10 Calibration curve used to determine the % amount of Aragonite in a Aragonite/Calcite coating mixture. The ordinate is computed by dividing the aragonite band area at 203.5 cm^{-1} to the calcite band area at 269.5 cm^{-1}.

It is noted that the above dry blending method is relatively straightforward and provides the best calibration curve when compared to other calibration methods. For example Figure 3.11 also includes a calibration curve generated from a stirred aqueous suspension of known quantities of Aragonite and Calcite. When compared to XPS data, we find that there is agreement between the dry blend calibration curves while the stirred aqueous suspension is in error. We attribute the error in the aqueous stirred suspension to the high sensitivity of Raman band position and shape to environmental conditions. In particular, the spectra in the liquid state produce bands that are broader than found in the solid mixture or on paper coating and this results in a difference in the two calibration curves.

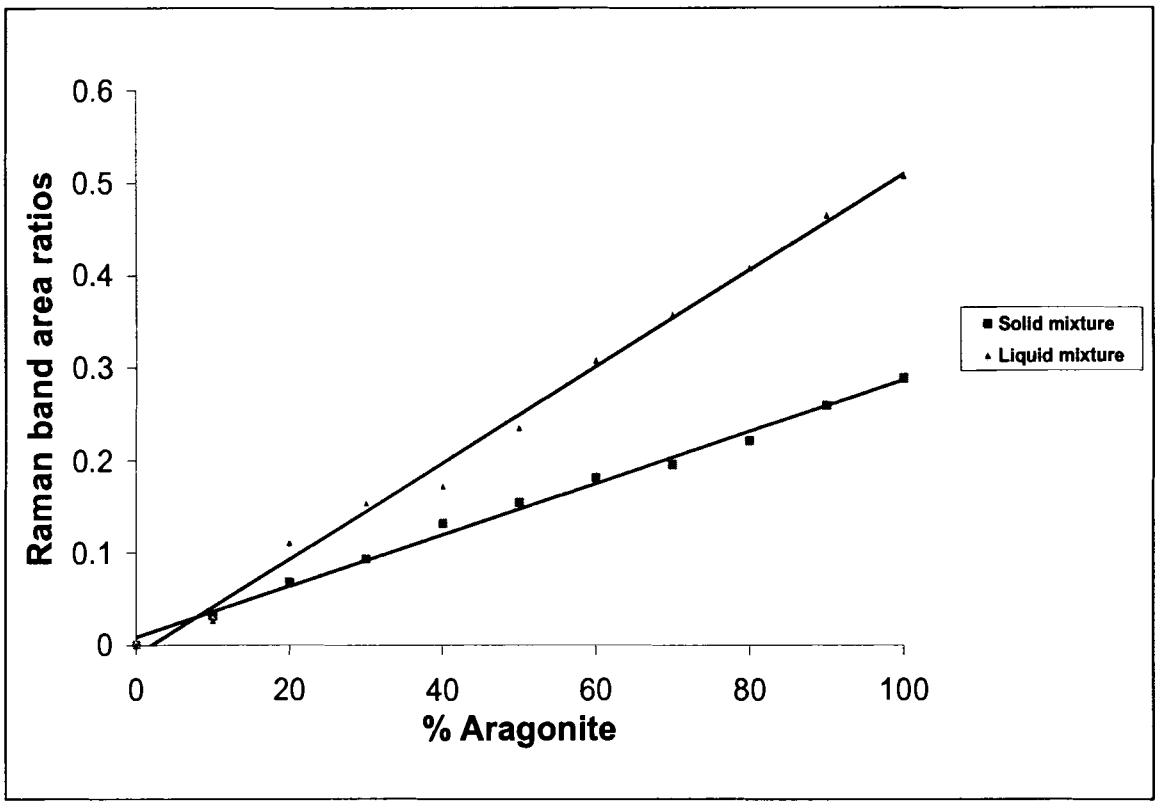

Figure 3.11 Calibration curves obtained from both liquid and solid Aragonite-Calcite mixtures.

3.4 Conclusion

Raman spectroscopy can easily detect the $CaCO_3$, anatase, rutile, styrene butadiene, and other coating components and can be used to distinguish the different morphology of $CaCO_3$ pigment, GCC and PCC. Kaolin based coatings have a large fluorescence background in its Raman spectrum and this doesn't prevent detecting other coating components. The investigation of paper coatings indicates that Raman spectroscopy can quantitatively detect $CaCO_3$ and styrene butadiene in paper coatings, with good reproducibility and these can be used to study the particle migration ($CaCO_3$, SB) phenomena in paper coatings.

Chapter 4

PARTICLE MIGRATION

4.1 Introduction

Coating color is a mixture of pigments, binders and additives, which have different particle sizes. When coating color is applied to paper, the wet coating is subjected to dewatering and coating penetration into the base paper. Since paper is a porous substrate made of cellulose fibers, dewatering begins at the moment of coating application due to water absorption through the fiber walls and capillary penetration into the pores of the base paper. Further liquid migration as well as coating penetration occurs due to hydrodynamic pressure at the applicator bar. These hydrodynamic pressures force all the coating ingredients to penetrate into the pores of the base paper, but pigments and particulate ingredients such as large latex particles tend to retain at the paper surface which acts as a filter. As the wet coating on the paper is heated and the liquid surface reaches the dew point, water will evaporate from the wet coating surface. Water lost at the liquid surface will be replenished by surface tension-driven convection and capillary, resulting in small particle (binder or pigment) migration toward the coating surface.

Therefore small particles may be carried with movement of the aqueous phase of coating colors toward the base paper during drainage or towards the surface during drying. This movement is a function of the water transport properties of the base paper (type of furnishes, the extent of refinement, the degree of sizing and the pore sizes), its dimensional changes that occur with wetting (fiber swelling and debonding), external pressures (compression and recovery), the properties of filter cakes, and the time of

contact. The extent to which the small particles migrate to the surface during the drying process depends on drying conditions, the wet coating structure, the type of small particles (other pigments, water soluble binders, latexes, etc.) and the physical, thermal and colloidal properties of small particles (particle sizes, filming-forming properties, colloidal stability, etc).

We have limited our study to the particle size differences. For this study, a pigment/binder system and a pigment/pigment system are considered.

4.2 Approach

Table 4.1shows the three different sizes of pigments (large - 2.3 μm, medium - 0.65 μm, small- 0.3 μm) mixed with a combination of SB latex binder (DOW 620 NA, size – 150 nm). Coating colors are then applied on the three base sheets, light weight coated (LWC), sized wood free base sheets (80 gsm, Hansol) and plastic film (Mylar, Dupont). LWC base sheet is a high absorbing material where as Plastic film is a non-absorbing polymer material. The sized paper does absorb water slowly. Ahn and Bousfield (2002)[56] characterized the LWC and Sized sheets, labled B3 and B1 respectfully. In some set of experiments ink jet photo paper is also used along with these base sheets. Ink jet paper (Brochure & flyer paper, two side coated -160 g/m^2, Hewlett-Packard) has greater absorbing capacity than that of LWC base sheet. These base sheets are chosen to see the effect of dewatering and evaporation on the composition of the coatings.

Table 4.1 Pigment-Binder System

Pigment ($CaCO_3$)		Binder		Coating color
Large (2.3 μm)				Applied on
Medium (0.65 μm)	+	SB latex (150 nm)	⟶	LWC, sized,
Small (0.3 μm)		(DOW 620NA)		Plastic film

In Pigment-Pigment system, two Aragonites (0.4 μm, 0.6 μm) and two Calcites (1.2 μm, 2.3 μm) are mixed in the way shown in Table 4.2. Same base sheets are coated for pigment migration analysis.

Table 4.2 Pigment-Pigment System

Pigment ($CaCO_3$)		Pigment ($CaCO_3$)		Coating color
Aragonite (0.4 μm)		Calcite (2.3 μm)		Applied on
Aragonite (0.6 μm)	+	Calcite (2.3 μm)	No Binder ⟶	LWC, sized,
Aragonite (0.4 μm)		Calcite (1.2 μm)		Plastic film,
				Ink jet Photo paper

4.3 Results and Discussion

Coating colors are prepared of various levels of binders (5 pph, 10 pph and 20 pph) with pigments of (large - 2.3 μm, medium - 0.65 μm, small- 0.3 μm). Coating color preparation and application on the base sheets are explained in chapter 2. Coating colors are applied on LWC, Sized and Plastic film using rod draw down coater and the surface

of all these coated sheets are scanned using the Raman Spectroscopic system (Renishaw 1000). Ratio of peak intensities of SB and $CaCO_3$ are calculated for each coated sheet and average SB/$CaCO_3$ ratios are plotted with binder amounts. 10 different points are scanned for each base sheet and an average is calculated. Throughout this thesis an SB/$CaCO_3$ ratio refers to average SB/$CaCO_3$ ratio. Same is applicable to reported pigment concentration on coated sheets.

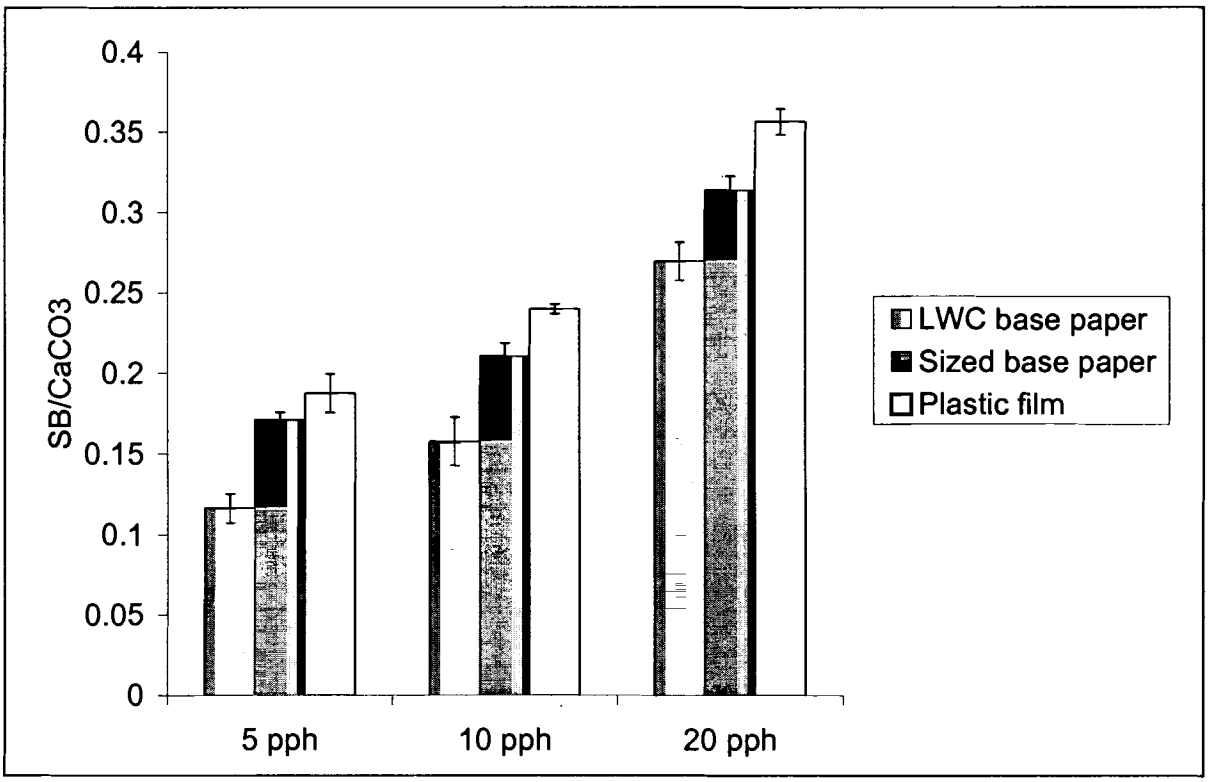

Figure 4.1 SB/$CaCO_3$ Raman band peak area ratios plotted against binder concentrations using a $CaCO_3$ of 2.3 μm size

Figure 4.1 shows average SB/$CaCO_3$ ratio for various binder amounts with the 2.3 μm $CaCO_3$ pigment particle. Pore sizes and pore volume created by these large pigments of 2.3 μm facilitates the movement of finer SB latex towards the paper during dewatering

of coating color. This depletes the binder on the surface resulting in less SB/$CaCO_3$ ratio on LWC and sized compared to Plastic film. On Plastic film, there is no dewatering and evaporation dominates which results in high concentration of finer SB particles at the surface. At higher binder concentrations in the coating color, there is more binder migration and thus more depletion of binder at the surface. Thus the difference in SB/$CaCO_3$ ratio between LWC and Plastic film increases as the binder level in the coating color increases.

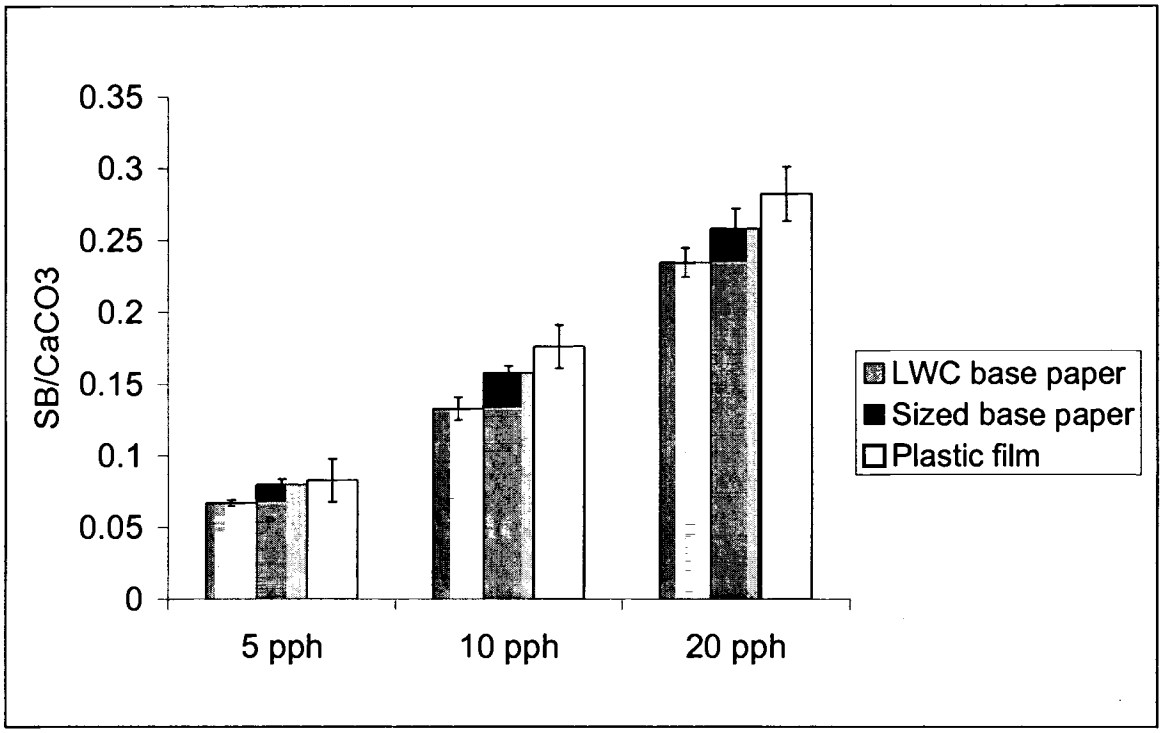

Figure 4.2 SB/$CaCO_3$ Raman band peak area ratios plotted against binder concentrations in a $CaCO_3$ of 0.7 μm size

Figures 4.2 and 4.3 show SB/$CaCO_3$ ratio at different binder amounts with a 0.7 μm and 0.3 μm $CaCO_3$ pigment particle. Pore sizes caused by these pigments are smaller relative to the 2.3 μm coating and therefore the movement of SB latex during dewatering

of coating color is not as pronounced. In other words, the depletion of SB binder on the surface is less when using 0.7 μm than 2.3 μm $CaCO_3$ in coatings. For the 0.3 μm pigment, little motion is detected for all cases.

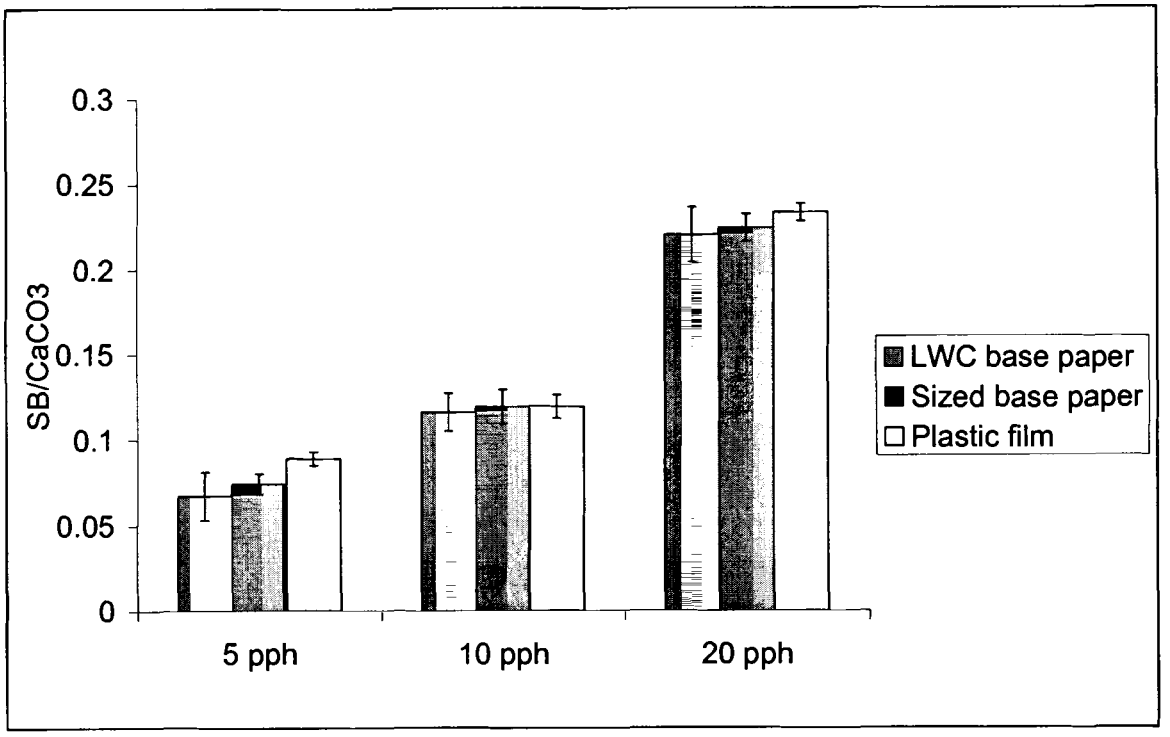

Figure 4.3 SB/$CaCO_3$ Raman band peak area ratios plotted against binder concentrations in a $CaCO_3$ of 0.3 μm size

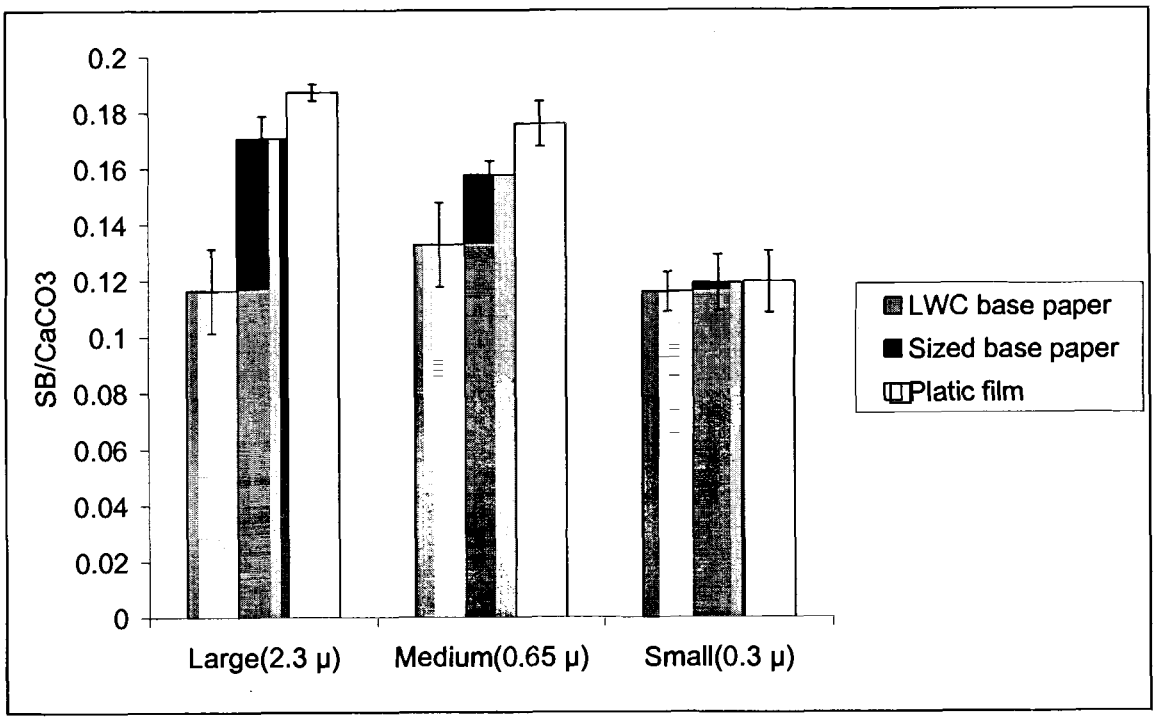

Figure 4.4 SB/$CaCO_3$ Raman band peak area ratios plotted against different sizes of $CaCO_3$ pigment

Figure 4.4 shows SB/$CaCO_3$ ratio plotted with pigment sizes. SB/$CaCO_3$ ratio difference between LWC and Plastic film decreases from large pigment coating color to small pigment coating color. Large pore sizes created by large pigments allow more binder to migrate during dewatering on LWC thus depleting binder at the surface and causing large difference of SB/$CaCO_3$ ratio between LWC and Plastic film. For small pigments, the pore size is smaller and the difference of SB/$CaCO_3$ ratio between LWC and Plastic film diminishes. Figure 4.5 depicts the binder migration phenomena among the three pigment sizes.

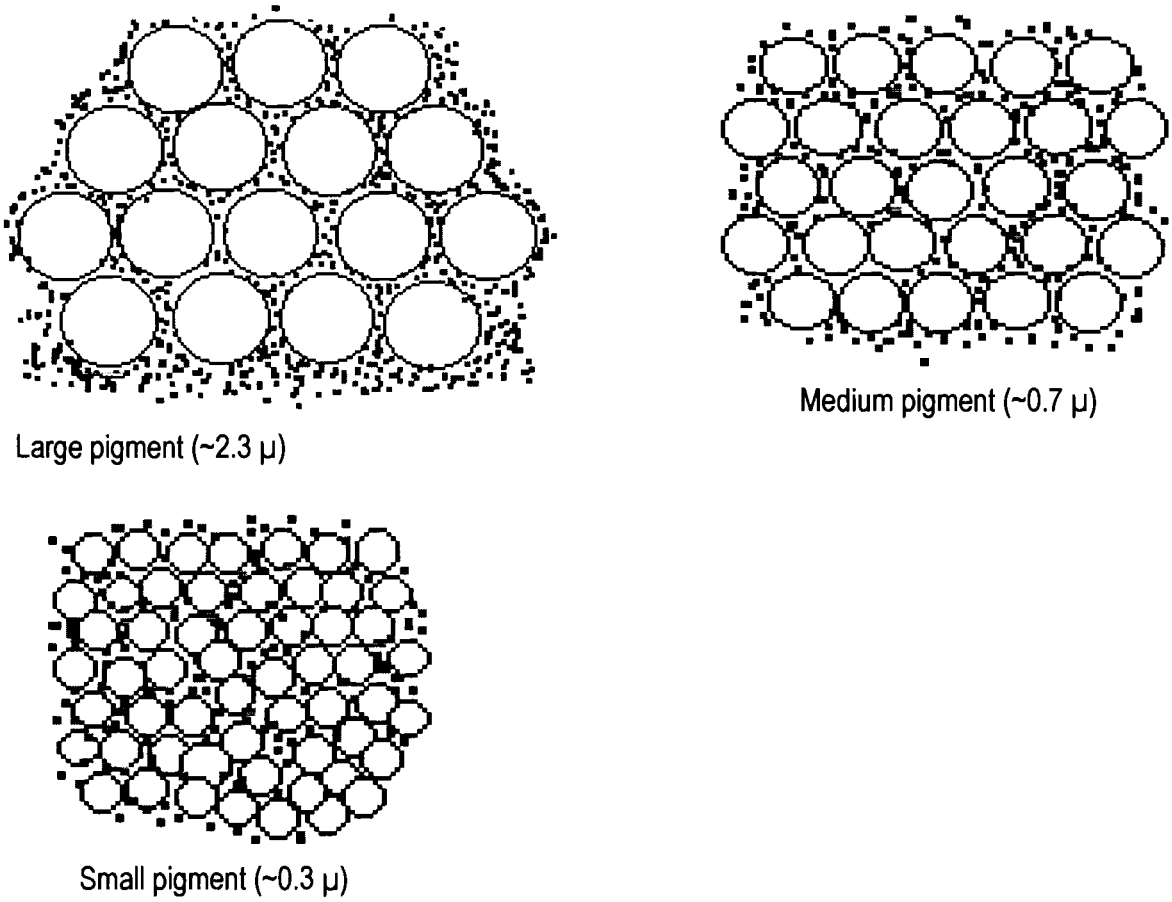

Figure 4.5 Binder migration phenomena among the three pigment sizes.

The large pores of 2.3 μm pigments allow more binder to migrate causing binder depletion on the coating surface. Pore sizes decrease with pigment size which in turn decreases binder migration. This continues until the critical point where the pore size almost becomes the size of the binder.

Pigment/binder size ratios are calculated in Table 4.3 to estimate the critical point where the binder migration starts in the pigment-binder systems. Migration of SB latex becomes significant when the pigment/binder size ratios are between 2 and 4.66. This is

close to the expected pore size generated by the pigment system. Lee (1983) [57] showed that the pore size should be close to $1/3^{rd}$ of the particle size for particle migration to occur. Therefore, this critical migration ratio is near the expected ratio where the binder is close to the pore size.

Table 4.3 Pigment/Binder Size Ratios

Pigment	Binder	Pigment/Binder size ratio	Binder migration
Small (0.3 μ)	150 nm	2	NO
Medium (0.7 μ)	150 nm	4.66	YES
Large (2.3 μ)	150 nm	15.33	YES

CMC (Carboxy methyl cellulose) is known as a water retention additive. 0.1 pph of CMC is added to the 10 pph coating color containing pigment of 2.3 μm size. CMC flocculates the binder molecules creating large size particles of SB. Even though the coating color is made of the large $CaCO_3$ pigment, Figure 4.6 shows that the SB latex is reduced. Therefore we see almost the same SB/$CaCO_3$ ratios on all the three base sheets irrespective of their absorbing capacity.

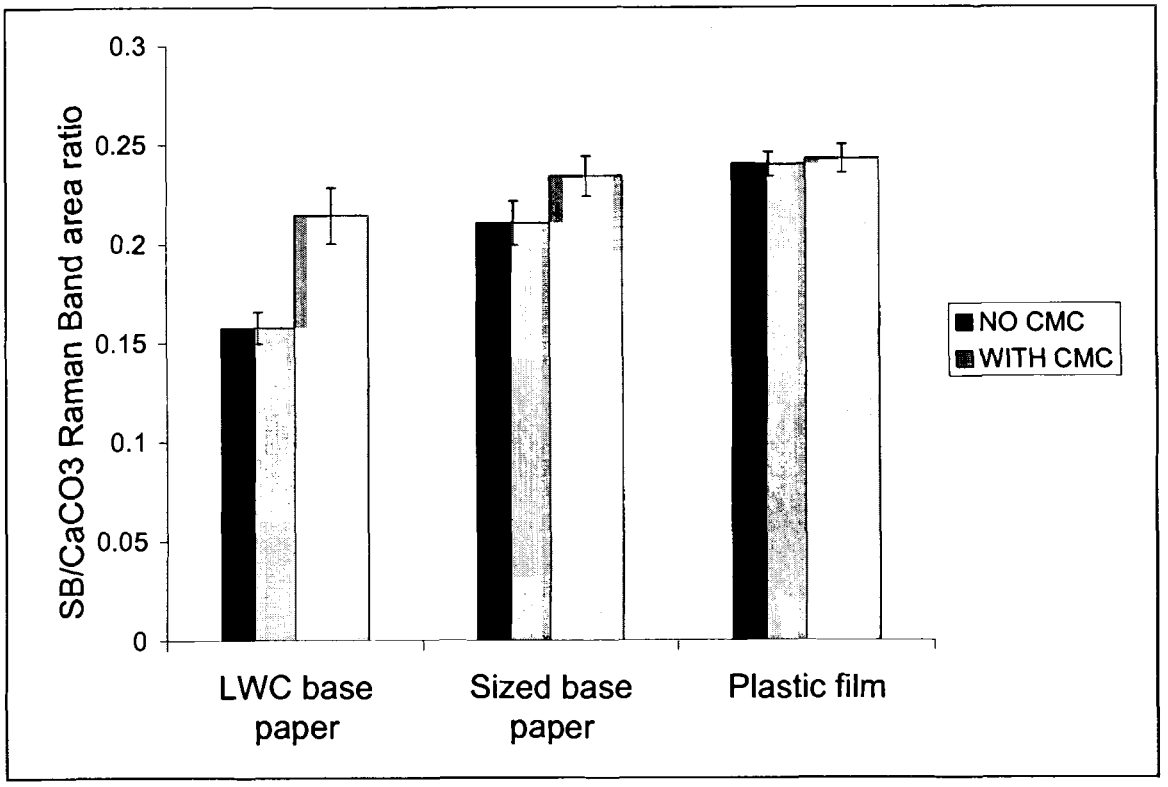

Figure 4.6 $SB/CaCO_3$ Raman band peak area ratios plotted against base sheets with CMC in coating color

A 50/50 (% wt) mixture of Aragonite (small-0.4 μm) and Calcite (large-2.3 μm) is prepared and coated on base sheets. Calibration curve for this pigment-pigment system is constructed as outlined in chapter 3 and used to find the percent Aragonite from the Aragonite-Calcite peak ratios. As seen in the following figure 4.7, percent Aragonite on LWC is decreased from original 50 % where as greater than 50 % concentration is found on Plastic film.

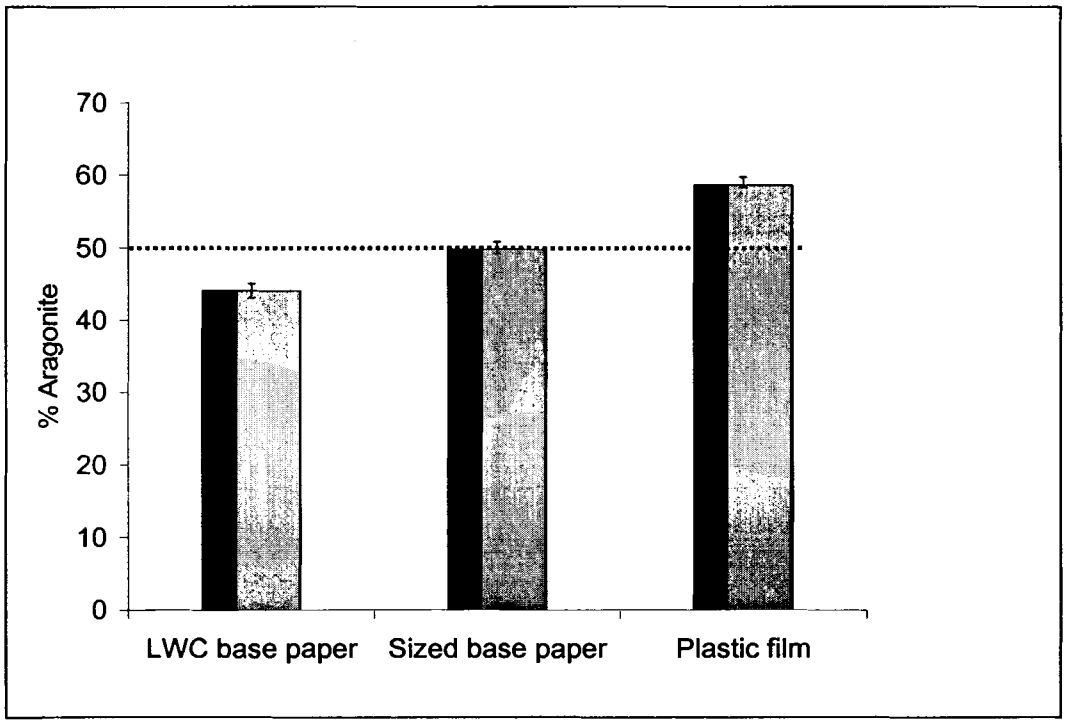

Figure 4.7 Aragonite concentrations for a 50/50 mixture applied on various substrates.

LWC being an absorbing substrate cause small Aragonite particle migration in the dewatering stage and hence depletion of Aragonite to 41% from original 50 % (wt). The increase in % Aragonite on Plastic film can be accounted for the sedimentation of large Calcite particles leaving a surface layer of relatively large concentration of small Aragonite particles. As calculated by Stoke's equation, a 2.3 μm particle takes only 2.03 sec to travel 10 μm distance in water. Therefore on Plastic film, the large Calcite particles deplete from the top layers causing an increase in the Aragonite concentration as depicted in Figure 4.8.

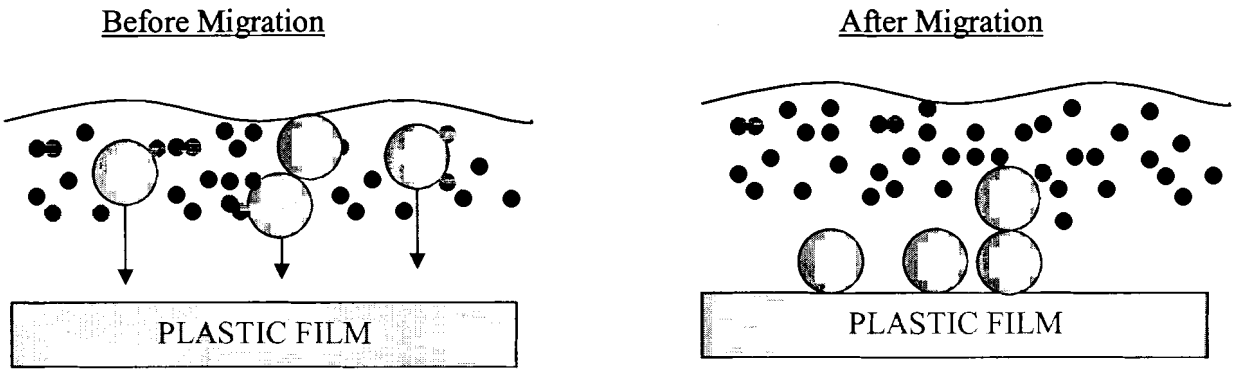

Figure 4.8 Large calcite particle sedimentation on Plastic film.

Stoke's equation for the terminal velocity of a sphere is given by

$$U_t = \frac{g * D_p^2 * (\rho_p - \rho)}{18 * \mu}$$

Where D_p is diameter of the particle, μ is viscosity and ρ_p and ρ are the densities of the particle and fluid, and g is the acceleration of gravity. Table 4.4 lists the settling time for various pigment sizes for coating layer thickness of 10 μm.

Table 4.4. Settling Time for Various Pigment Sizes

Pigment Size (μm)	Settling Time (Sec)
2.3	2.03
0.65	25.42
0.3	119.34

In another size combination, Aragonite of 0.6 μm and Calcite of 2.3 μm is used for 50/50 pigment mixture. Again calibration curve is constructed for this system, as

explained in chapter 3, to calculate Aragonite concentration on the surface of coated sheets using the Aragonite-Calcite peak ratios. Aragonite has decreased on the LWC to only 46%, shown in figure 4.9, when compared to the previous case of (0.3μm Aragonite) 41% from 50%. The reason for this difference is that, large Calcite pigments still forms the same size pores but, in this case, there is less migration of the 0.6 μm fine pigment due to its large size.

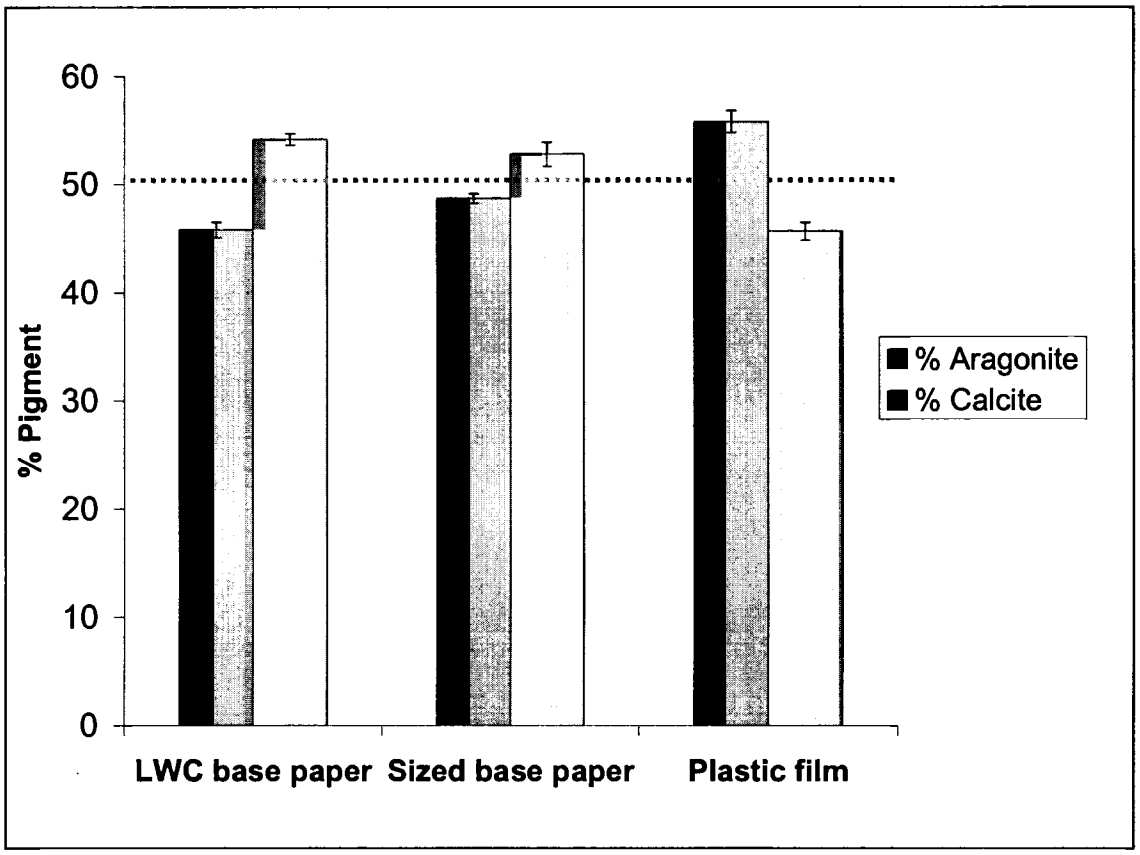

Figure 4.9 Pigment weight percentage for a 50/50 mixture of Aragonite (0.6 μm) and Calcite (2.3 μm) applied on various substrates.

Figure 4.10 shows slight/no change in Aragonite concentration on the surface with a pigment-pigment mixture containing 50/50 (% wt) of even large Aragonite (0.4 μm) and Calcite (1.2 μm).

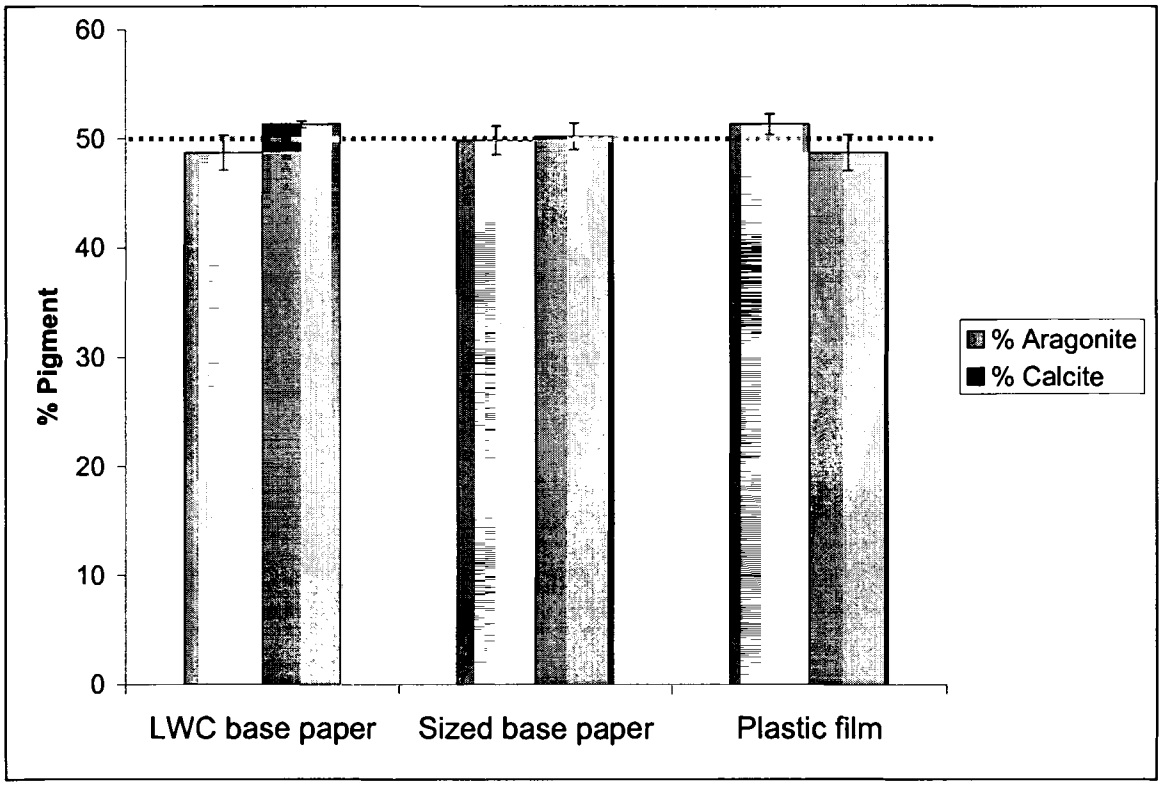

Figure 4.10 Pigment weight percentage for a 50/50 mixture of Aragonite (0.4 μm) and Calcite (1.2 μm) applied on various substrates.

Pigment/pigment size ratios for all the above three cases are listed in Table 4.5. When the Calcite/Aragonite size ratio is less than 3, there is no significant particle migration. For ratios larger than 3, there is motion, even sometimes on plastic films because of sedimentation.

Table 4.5 Pigment/Pigment Size Ratios

Pigment	Pigment	Size Ratio	Fine Pigment Migration
Aragonite (0.4 μ)	Calcite (2.3 μm)	5.75	YES
Aragonite (0.7 μ)	Calcite (2.3 μm)	3.28	YES
Aragonite (0.4 μ)	Calcite (1.2 μm)	3	NO

The Aragonite/Calcite compositions are changed from 50/50 (% wt) to 25/75 (% wt). Also, a highly absorbent sheet ink jet paper is used in addition to LWC, sized and Plastic film. For a combination of Aragonite (0.6 μm)/Calcite (2.3μm), the Aragonite and Calcite concentration on the surface of the coated sheets is calculated from a calibration curve and is shown in Figure 4.11 (front row)

Use of high concentration of large Calcite pigment increases the percentage of large pores in the coating layer. Therefore more Aragonite is depleted on absorbing sheets like ink jet and LWC sheets. The decrease of Aragonite on LWC is higher in this case compared to the decrease obtained with that of 50/50 mixture.

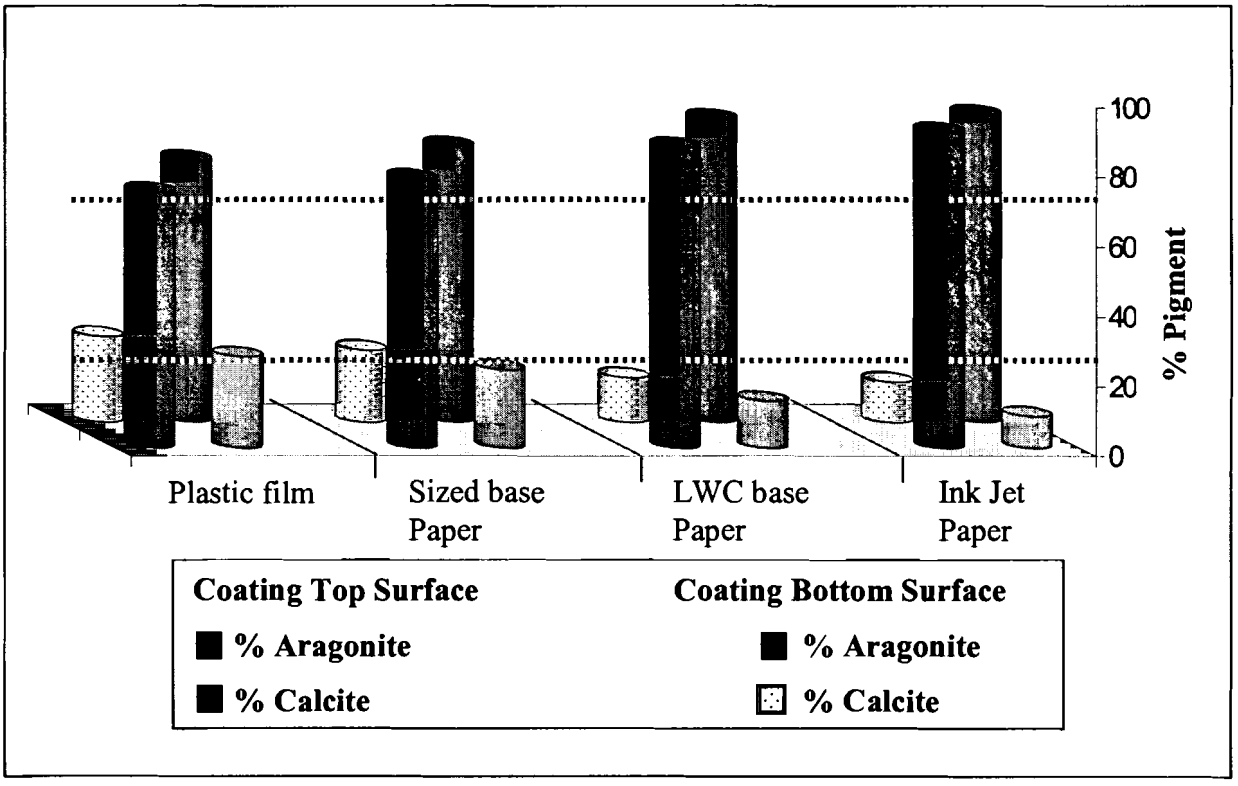

Figure 4.11 Pigment concentrations (Aragonite and Calcite) on the top and bottom surface of coating layer.

Recording the Raman spectra on the backside of the coating layer provides additional evidence of pigment migration. These coatings are peeled off (as they are non-binder coating layers) from base sheets and a complimentary profile of Aragonite to that of top surface is found as given in Figure 4.11 (back row). These results validate the procedures because they show the quantitative increase or decrease.

4.4 Conclusion

The results show that binder migration depends on the pigment/binder size ratio and not the absolute concentration of binder in the coating color. Furthermore, paper coatings with higher pigment/binder size ratios show higher binder migration. The role of CMC is to aggregate the binder and this lowers the pigment/binder size ratio, which in turn reduces binder migration. The results indicate that pigment migration is a result of size differences and not that of surface chemistry for the systems studied. For the Calcite/Aragonite systems, Raman Spectroscopy seems to be the only method to study these cases.

Chapter 5

COATING NON-UNIFORMITY & PRINT MOTTLE STUDIES WITH RAMAN SPECTROSCOPY

5.1 Introduction

In chapter 4, we showed that Raman spectroscopy can be used to characterize coatings in terms of pigment/binder and pigment/pigment distribution. For these measurements, an average of 10 points was collected from various locations on the paper coating to calculate pigment/binder and pigment/pigment ratios characteristic to that coating. In this chapter, we now want to quantify the contribution of the non-uniformity in the spatial composition of the paper coating to various print defects such as 'mottle'. To achieve this goal, we first show that we can detect spatial differences in pigment/binder ratios in the non-uniform base sheets. Next, we identify the key Raman bands of inks and show that they do not overlap with the coating components key bands. Finally, we examine the print defects together with pigment/binder spatial composition of the coating.

5.2 Non-Uniform Absorption of Base Sheets

The LWC and sized sheets are printed with toner spots of 2 mm diameter by a laser jet printer (Laser Jet 4050N, Hewlett-Packard). Then 25/75 Aragonite (0.6 μm)/Calcite (2.3 μm) pigment mixture is applied on these base sheets. Figure 5.1 show that areas above toner spots contain a higher Aragonite composition as compared to non-toner spots on the LWC base. The toner spots are a polymer film, which prevent

dewatering from the coating color as opposed to non-toner spots. There is still some depletion of the fine particles over the spots on LWC. The difference is minimal on the sized sheet. Plastic film was also printed for toner spots but they were spreading. Therefore, data from plastic film are not compared with LWC and sized sheets.

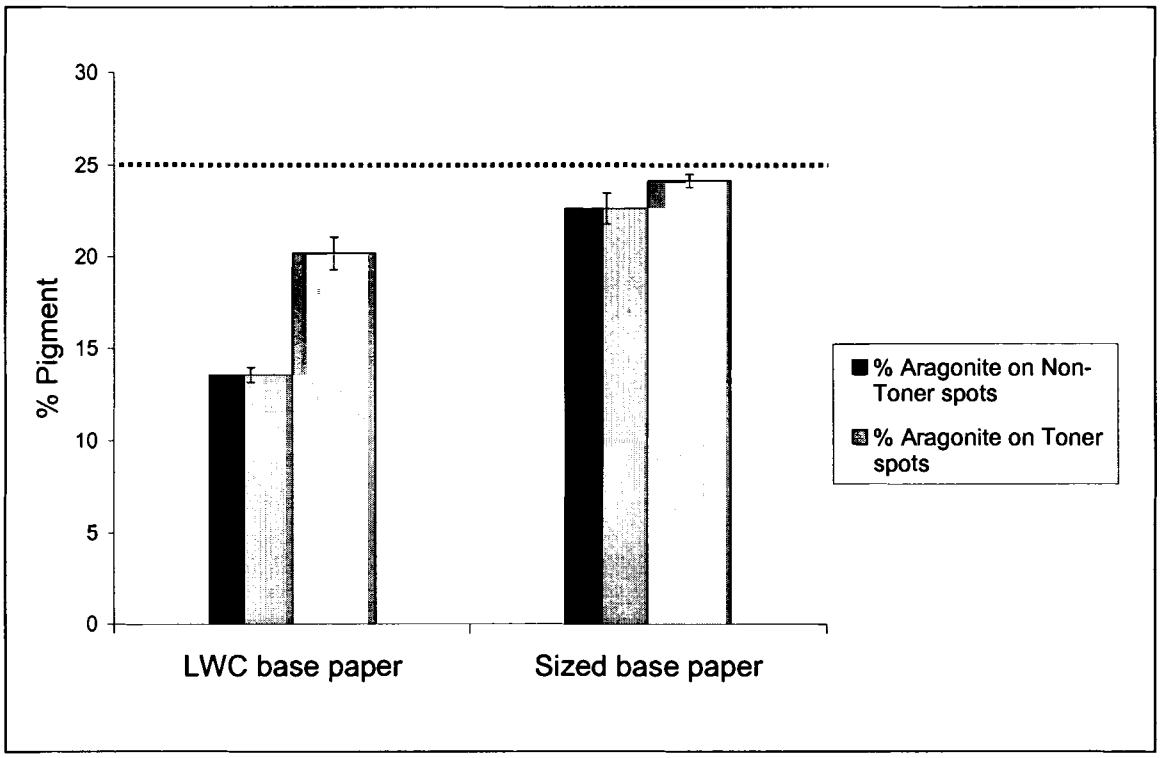

Figure 5.1 Small Aragonite pigment concentrations over toner and non-toner spots on LWC and sized substrates.

Use of toner spots to illustrate the non-uniform absorption of base sheets may be an extreme case but a base paper with variation in absorption of the coating components results in similar non-uniform spatial composition. Large differences between the spatial pigment/binder compositions result in a non-uniform absorption of ink producing mottle.

5.3 Inks

Raman spectra of three ink jet inks (cyan, magenta, and yellow) are shown in figure 5.2

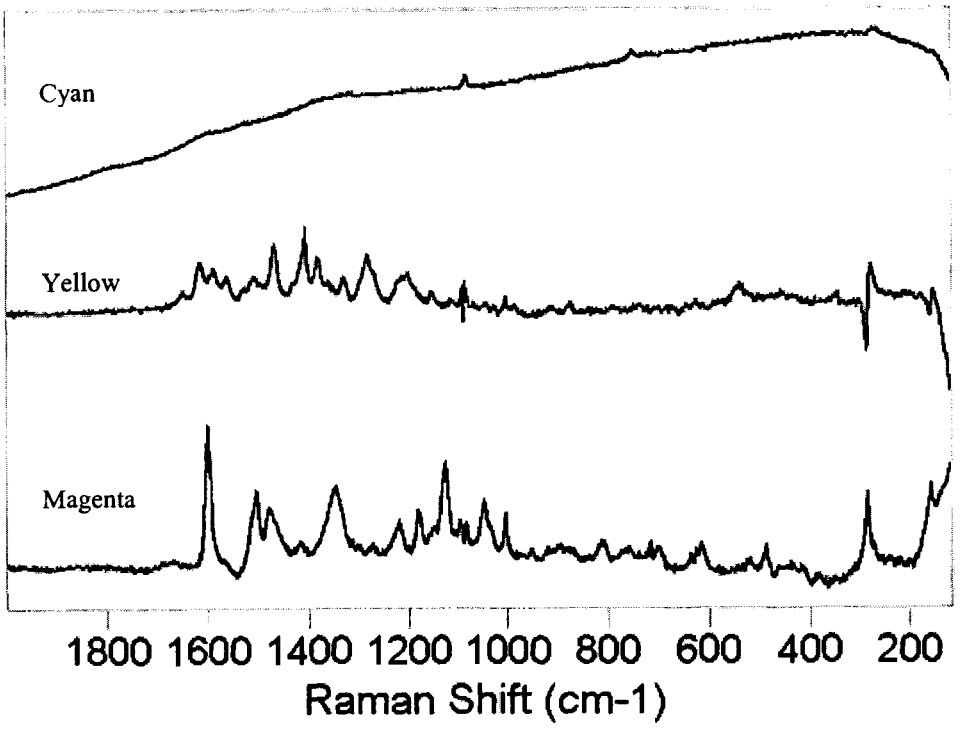

Figure 5.2 Raman spectra of yellow, magenta, and cyan inks.

From the spectra we can see that magenta and yellow inks give rise to distinctive Raman bands, where as cyan ink is difficult to detect because of fluorescence background. Magenta ink has a characteristic band at 1599 cm^{-1}. Yellow ink has several identifiable bands from 1600 cm^{-1} to 1200cm^{-1}, such as the band at 1465 cm^{-1}. There is minimal fluorescence with yellow inks using our 785 nm based system. Yellow ink is chosen for print mottle studies because there are no bands below 1200 $cm^{-1}$to overlay with $CaCO_3$ (1096 cm^{-1}) and SB latex (1001 cm^{-1}) Raman bands. This is shown in Figure 5.3 which is the Raman spectra of printed sheet with yellow ink on $CaCO_3$ -SB coating.

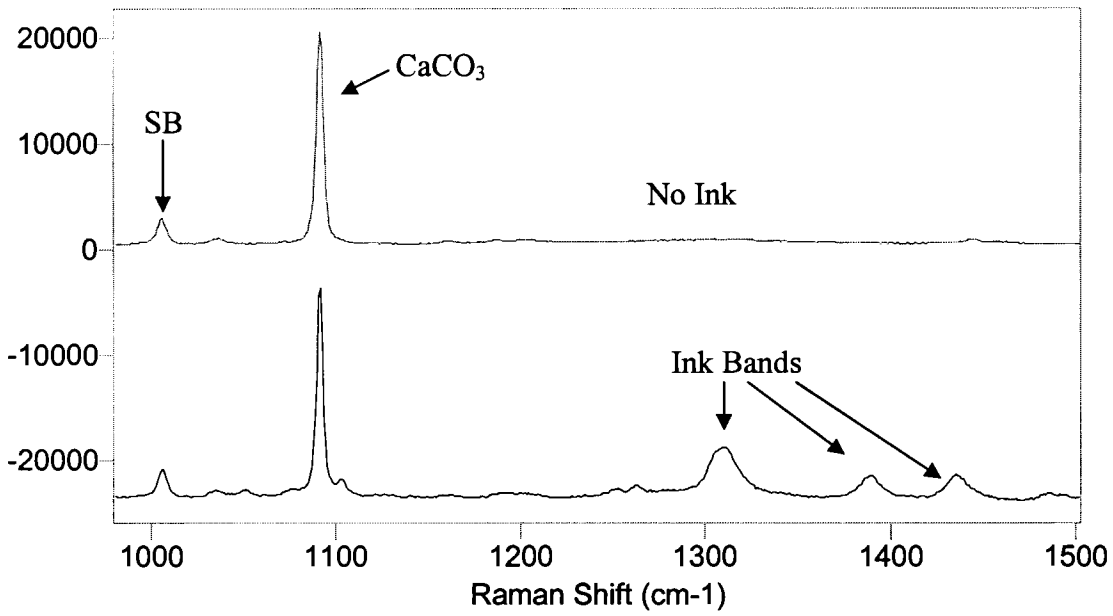

Figure 5.3 Raman spectra of a $CaCO_3$-SB coating with and without pigmented yellow ink.

5.4 Print Mottle

Mottle is defined as the unevenness in print density or print gloss. The appearance of ink on coated sheets is controlled by two factors - absorptivity of the ink vehicle into the coated surface and smoothness of coated surface. In other words, non-uniform wetting and penetration of ink into substrate and surface tension properties of substrate affects the mottle. Print mottle can be a small variation in either gloss or color. It can also occur in solids, half tone areas, or both. Calendaring and wet pressing is done on coated sheets to make them smoother sheets so that the ink coverage will be uniform. Generally, Tobias Mottle Tester (MTI) is used to measure the mottle. MTI measures the mottle by measuring the variation in reflective density of a sample at controlled ink film thickness.

In our experiments, both dye yellow ink and pigmented yellow ink are applied on coated sheets using a Bristow wheel. This device is good to characterize absorption rates.

Though we are not measuring the absorption rates, we have used it to apply inks on to the coated sheets. The instrument, as shown in Figure 5.4, consists of a wheel, which can rotate at a fixed speed. A rectangular strip of the media (coated sheet) is attached to the rotating wheel, and a known amount of ink (10 μL) is applied to the coated sheet through the ink trough, which holds the ink by surface tension.

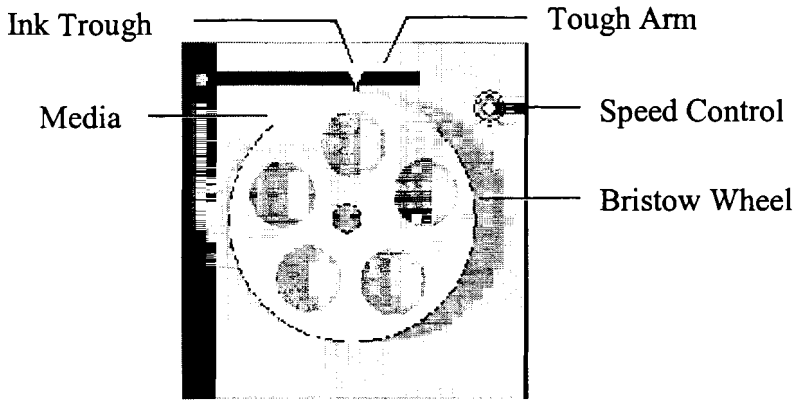

Figure 5.4 Bristow wheel (Side View)

Sized base sheets are coated with a 10 pph SB latex $CaCO_3$ (0.7 μm) and taped to the Bristow wheel. Pigmented yellow ink is applied at a speed of 0.3 cm/s and the image of the printed sheet is shown in the Figure 5.5.

5.5 Results and Discussion

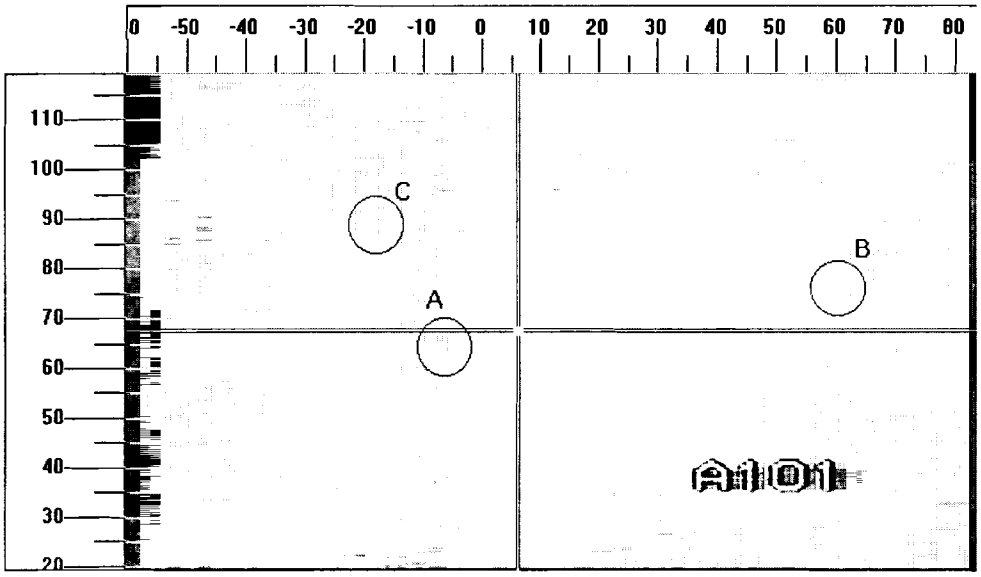

Figure 5.5 Raman Image of printed sheet. Pigmented yellow ink is applied on $CaCO_3$-SB coating using Bristow wheel at 0.3 cm/s.

Three areas of varying ink densities (dark - A, medium - B and light - C) are considered and 10 points are scanned within the circles indicated above (A, B, C). Band intensities of $CaCO_3$ and SB at 1096 cm^{-1} and 1001 cm^{-1} respectively are calculated as explained in chapter 3 and SB/$CaCO_3$ ratios are plotted for different ink concentration areas in Figure 5.6.

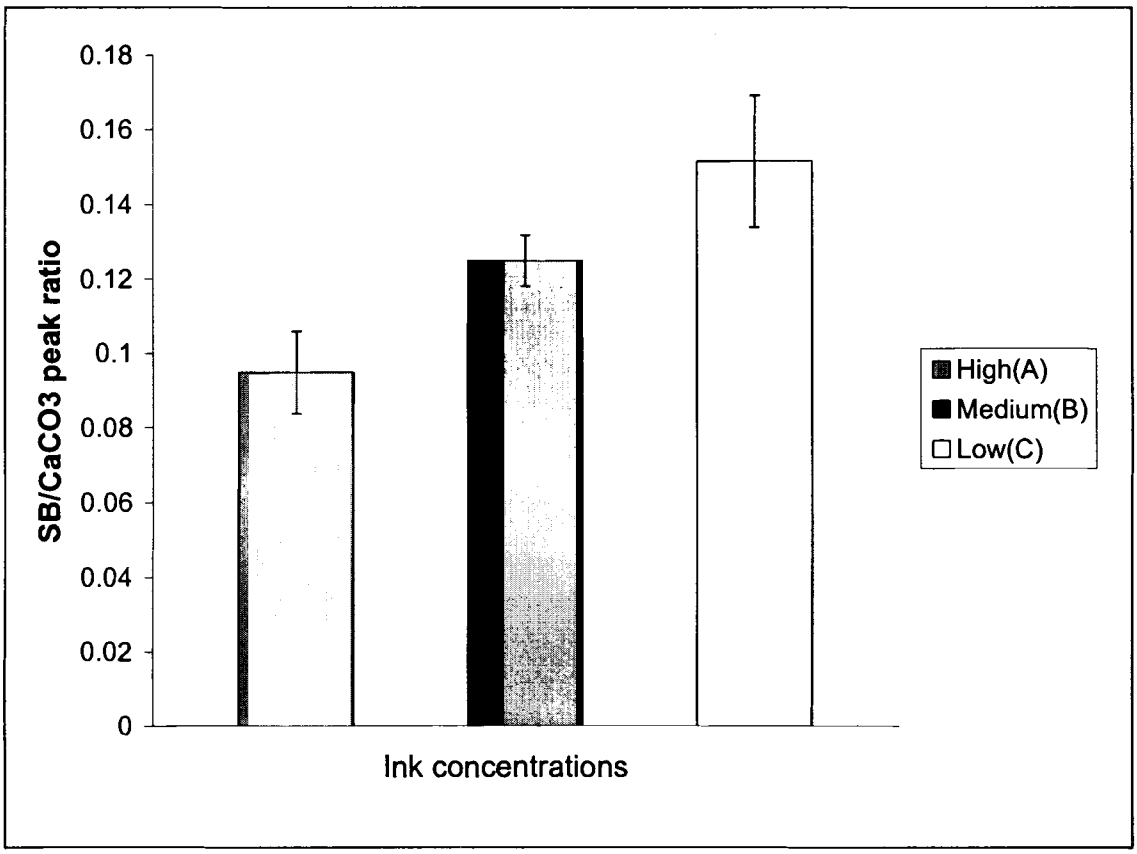

Figure 5.6 $SB/CaCO_3$ peak ratios for print mottle.

As we see from figure 5.6, low $SB/CaCO_3$ results high ink density where as high $SB/CaCO_3$ results in the opposite. Low SB concentrations are expected to cause that area to be more porous which allows more ink to penetrate in that area. When more ink vehicle is absorbed, it leaves ink pigment particles on the surface and thus produces higher ink density. In contrast, higher SB concentration at the surface results in less ink density on coating. This mechanism is shown in figure 5.7. Most industrial printing processes currently use pigmented inks. Though we cannot characterize the uniformity of absorption in the base sheet, we expect that regions of high absorption could cause a coat layer region low in SB latex concentration, from the results in chapter 4.

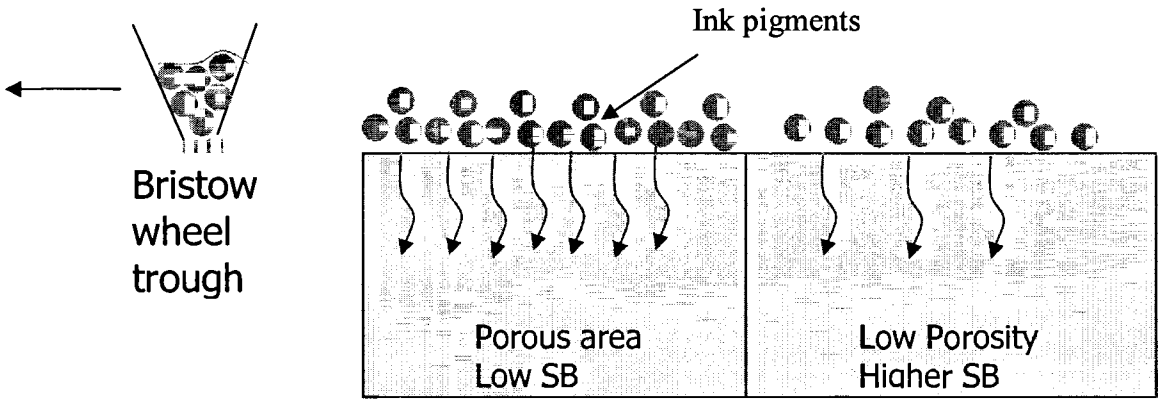

Figure 5.7 Pictorial representation of print mottle for pigmented ink on $CaCO_3$-SB coatings.

Though the ink in this case is deposited in a controlled way and it is water based, the same type of mechanisms may act in conventional printing. For offset lithographic printing, rapid absorption on spot may lead to a higher ink density in a rolling nip geometry with a film split.

Yellow dye based ink is also applied on same coated sheet (10 pph SB latex $CaCO_3$ (0.7 μm on sized base sheet) using the Bristow Wheel and the image printed sheet is shown in the following Figure 5.8.

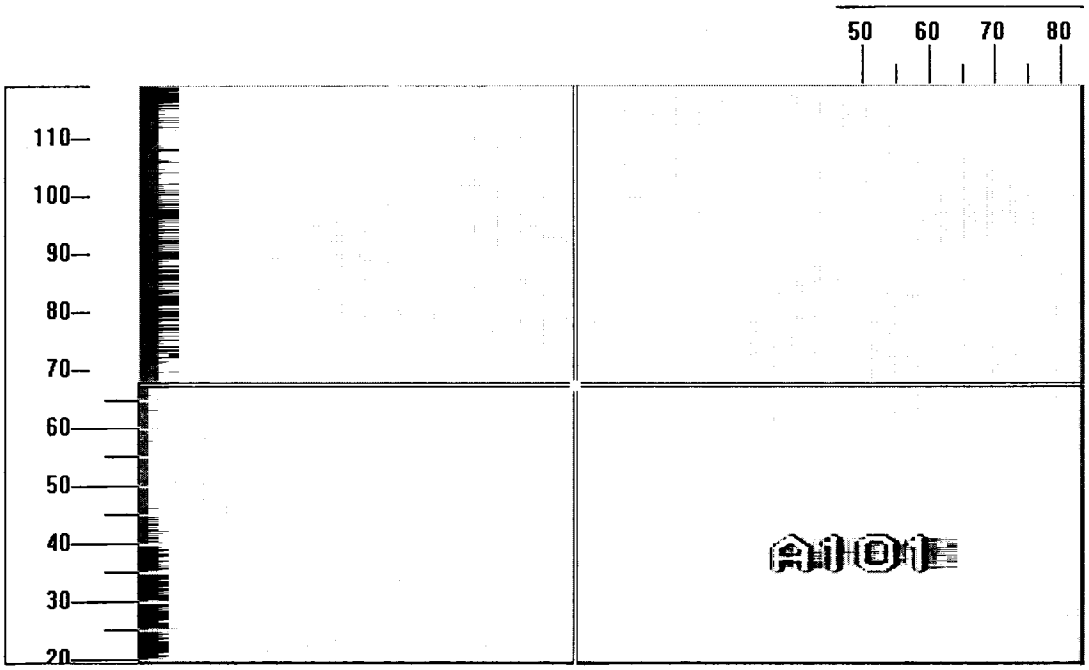

Figure 5.8 Raman image of printed sheet. Yellow dye based ink is applied on $CaCO_3$-SB coating using Bristow wheel at 0.3 cm/s.

As we see in the above figure, it is difficult to locate the mottled regions visually with varying ink densities. Many regions are scanned and we found that the differences between SB/$CaCO_3$ are minimal and we can't explicitly relate those small differences to the mottle. For dye based systems, the dye molecules can penetrate deep into the coating layer. Therefore, even though no mottle is present to the eye, uneven absorption could have taken place.

5.6 Conclusion

Point-to-point variations in the base sheet absorption can lead to variation in coating layer composition. Non-uniform distribution of pigment/binder composition in coatings leads to print mottle generation for pigment inks. Low amount of binder leads to high density of ink because high absorption regions deposit more ink pigments.

Chapter 6

SUMMARY

6.1 Conclusions

The major conclusions that can be drawn from this thesis are

- The subtle differences between Ground Calcium Carbonate (GCC) and Precipitated Calcium Carbonate (PCC) can be detected and quantified using Raman spectroscopy.
- Raman spectroscopy can distinguish and quantify different morphologies of $CaCO_3$, Calcite and Aragonite.
- Dry blends of the coating components to record spectra yields good calibration curves.
- For Pigment/Binder systems, binder migration depends on the pigment/binder size ratio and not on the absolute concentration of binder in the coating color. Similar results are observed with pigment-pigment systems.
- A critical size ratio greater than three is found necessary for particle migration to occur.
- Carboxy Methyl Cellulose (CMC) reduces binder migration for the systems studied.
- Raman spectroscopy can quantify the contribution of the non-uniformity in the spatial composition of the paper coatings to generation of print mottle for pigmented inks.

- Large binder/pigment compositions contribute to low density of pigmented ink applied with a contact device.

6.2 Recommendations for Future Work

Throughout this research, particle distribution has been studied with $CaCO_3$ pigments and SB latex binder. Also only yellow ink was used because of the fluorescence limitations. For the conclusions to hold true for general cases, there is necessity to expand this work with even more real systems. Therefore the following recommendations are suggested for future work.

- Acquire UV laser to record fluorescence free spectra of kaolin clay, cyan and magenta inks. Then particle migration studies can be extended to $CaCO_3$-Clay systems which are more close to industrial samples.
- Investigate the effect of other additives on the critical migration ratio.
- Use characterized solutions instead of inks that can be easily detected and monitored by Raman spectroscopy, to study the absorption behavior of coated sheets.
- Extend the study of particle migration to different pigment shapes.
- Modify pigment surface chemistry and study its effect on the pigment/binder distribution.

REFERENCES

1. Lepoutre, P. *Prog. Org. Coat.* **1989**, *17*, 89-106.
2. Al-Turaif, H.; Bousfield, D. *Tappi J.* **2002**, *in press.*
3. Browning, B. L. *Analysis of Paper, 2nd Ed., Revised and Expanded* Marcel Dekker: New York, **1977**.
4. Arnold, M.; Oftringgen, P-S, AG *Ground Calciumcarbonate in Coated Papers and Board* OMYA Inc. **2001** [Online]. Available: http://www.omya.com/omya.nsf/frameset-paper?OpenPage (2002, June 11).
5. Osterhuber, E. *Tappi Coating Materials & Technologies Tutorial Conference.* May **2000**, Washington, DC.
6. Swalen, J. D.; Allara, D. L.; Andrade, J. D.; Chandross, E. A.; Garoff, S.; Israelachvili, J.; McCarthy, T. J.; Murray, R.; Pease, R. F.; Rabolt, J. F.; Wynne, K. J.; Yu, H. *Langmuir* **1987**, *3*, 932-950.
7. Kane, R. J. *Aqueous Paper Coatings* Tappi Press: Atlanta, **1995**.
8. Kane, R. J. *Paper Coating Additives* Tappi Press: Atlanta, **1995**.
9. Arai, T.; Yamasaki, T.; Ogawa, S.; Ogura, T. *TAPPI Coating Conf. Proc.* **1988**, 187-192.
10. Tomimasu, H.; Yamasaki, T.; Ogawa, S.; Ogura, T.; Sakai, Y. *TAPPI Coating Conf. Proc.* **1986**, 35-43.
11. Dappen, J. W. *Tappi J.* **1951**, *34*, 324-335.
12. Heiser, E. J.; Cullen, D. W. *Tappi J.* **1965**, *48*, 80A.
13. Eames, A. C. *Tappi J.* **1960**, *43*, 2.

14. Dupuy, N.; Ruckebush, C.; Duponchel, L.; Beurdeley-Saudou, P.; Amram, B.; Huvenne, J. P.; Legrand, P. *Anal. Chim. Acta* **1996**, *335*, 79-85.

15. Deley, J. P.; Gigi, R. J.; Liotti, A. J. *Tappi J.* **1963**, *46*, 188A-192A.

16. Dupuy, N.; Duponchel, L.; Huvenne, J. P.; Legrand, P. *Proc. SPIE-The Intl. Soc. Optical Eng.* **1993**, *2089*, 212-213.

17. Jiang, E. Y.; McCarthy, W. J.; Drapcho, D. L. *Spectros. Letters* **1998**, *13*, 21-40.

18. Wahls, M. W. C.; Kentta, E.; Leyte, J. C. *Appl. Spectrosc.* **2000**, *54*, 214-220.

19. Fujiwara, H.; Kline, J. E. *TAPPI Coating Conf. Proc.* **1987**, 29-34.

20. Kline, J. E. *TAPPI Coating Conf. Proc.* **1988**, 67-72.

21. Kline, J. E. *Tappi J.* **1991**, *74*, 177-182.

22. Whalen-Shaw, M.; Eby, T. *Tappi J.* **1991**, *74*, 188-191.

23. Ozaki, Y.; Sawatari, A. *Nord. Pulp & Pap. Res. J.* **1997**, *12*, 260-266.

24. Brinen, J. S. *Nord. Pulp & Pap. Res. J.* **1993**, *1*, 123-129.

25. Gron, J.; Dahlvik, P. *Nord. Pulp & Pap. Res. J.* **1998**, *13*, 119-123.

26. Brinen, J. S.; Proverb, R. J. *Nord. Pulp & Pap. Res. J.* **1991**, *6*, 47.

27. Brinen, J. S.; Proverb, R. J. *Nord. Pulp & Pap. Res. J.* **1991**, *6*, 177.

28. Hakkanen, H. J.; Korppi-Tommola, J.E.I. *Anal. Chem.* **1989**, *70*, 4724-4729.

29. Hakkanen, H.J.; Korppi-Tommola, J.E.I. *TAPPI Adv. Coating Fundamentals Sym. Proc.* **1999**, 191.

30. Dickson, R.; Forsstrom, U.; Gron, J. *TAPPI 2000 Coating Conf. Proc.* **2000**, 167-184.

31. Machula, G.; Dékány, I.; Nagy, L. G. *Colloids and Surf.* **1993**, *71*, 241-254.

32. Wendsjö, Å.; Thomas, J. O.; Lindgren, J. *Polym.* **1993**, *34*, 2243.

33. Snétivy, D.; Vansco, G. J. *Macromolecules* **1992**, *25*, 3320-3322.

34. Block, H.; Kelly, J. P. *J. Phys. D: Appl. Phys.* **1988**, *21*, 1661-1677.

35. Brandt, M. S.; Fuchs, H. D.; Höpner, A.; Rosenbauer, M.; Stutzman, M.; Weber, J.; Cardona, M.; Queisser, H. J. *Mater. Res. Soc. Symp. Proc.* **1992**, *262*, 849.

36. Smith-Palmer, T.; Lynch, B. M.; Roberts, C.; Lü, Y. *Appl. Spectrosc.* **1991**, *45*, 1022.

37. Schaeberle, M. D.; Morris, H. R.; Turner II, J. F.; Treado, P. J. *Anal. Chem.* **1999**, *71*, 175A.

38. Furo, I.; Daicic, J. *Nord. Pulp & Pap. Res. J.* **1999**, *14*, 221-225.

39. Prucker, O.; Rühe, J. *Mater. Res. Soc. Symp. Proc.* **1993**, *304*, 167.

40. Li, T.-Q.; Haggkvist, M.; Odverg, L. *Colloids Surf. A: Physicochem. Eng. Aspects* **1999**, *159*, 57-63.

41. Turrell, G.; Corset, J., Eds. *Raman Microscopy Development and Applications* Academic Press: London, **1996**.

42. Zlokarnik, G. *Anal. Chem.* **1999**, *71*, 322A.

43. Rezania, A.; Johnson, R.; Lefkow, A. R.; Healy, K. E. *Langmuir* **1999**, *15*, 6931.

44. Raman, C. V.; Krishnan, K. S. *Nature* **1928**, *121*, 50.

45. Placzek, G. *Handbuch der Radiologie* **1934**, *2*, 205.

46. Schawlow, A.; Townes, C. H. *Phys. Rev. A* **1958**, *122*, 1940.

47. Maiman, T. H. *Nature* **1960**, *187*, 493.

48. Porto, S.; Wood, D. L. *J. Opt. Soc. Am.* **1962**, *52*, 251.

49. Stoicheff, B. *Colloquim Spectroscopium Internationale* Spartan Books: Washington, DC, **1962**.

50. Vyorykka, V.; Halttumen, M.; Litti, H.; Kentta, E.; Passo, J.; Tenhumen, J.; Vuorinen, T.; Stenius, P. *TAPPI 2001 Coating and Graphic Arts Conf. Proc.* **2001,** 193-201.

51. *Renishaw Raman Imaging Microscope WiRE (User Guide)* Renishaw Plc., **1999,** 122-126.

52. Turrell, G.; Corset, J., Eds. *Raman Microscopy: Developments and Applications* Academic Press: London, **2000.**

53. Pei, H. *Raman Spectroscopy study of Paper Coatings,* master's thesis, Dept. of Chemistry, University of Maine, Orono, **2000.**

54. Murad, E.; Koster, H. M. *Clay Miner.* **1999,** *34,* 479-485.

55. Bower, D. I.; Maddams, W. F. *The Vibrational Spectroscopy of Polymers* Cambridge University Press: Cambridge, **1989.**

56. Seongnam, A.; Bousfield, D. *TAPPI Coating Conf. Proc.* **2002,** *in press.*

57. Van Gilder, R.; Lee, D. I.; Purfeerst, R.; Allswede, J. *Tappi J.* **1983,** *66,* 11-15.

BIOGRAPHY OF THE AUTHOR

Shivashanker Bitla was born on the 20th January, 1979 in Warangal, Andhra Pradesh, India. He graduated from S.S.N. Junior College, Ongole, Andhra Pradesh in May 1996. In 2000, he received his Bachelor of Engineering from University Department of Chemical Technology (UDCT), Bombay, India. He then moved to the United States of America to continue higher education. In September 2000, Shivashanker began his M.S. program in Chemical Engineering at The University of Maine.

During his graduate studies at The University of Maine, Shivashanker worked on the research project sponsored by the Paper Surface science program (PSSP) at the University of Maine. Shivashanker is a candidate for The Master of Science degree in Chemical Engineering from The University of Maine in August, 2002.